Terzaghi oration: Geotechnical aspects of the 1995 Kobe earthquake

Hommage à Terzaghi: Aspects géotechniques du tremblement de terre de Kobé de 1995

Kenji Ishihara – *Science University of Tokyo, Japan*

ABSTRACT The background information is given on the issues such as earthquake-generating plate tectonics in the Japanese archipelago, historical seismicity and development of fault rupture in the region of strong shaking during the Kobe earthquake. The geological setting and topography are described together with the expansion of land reclamation in the port area of Kobe. Characteristics of the ground motions recorded at various sites during the earthquake are also presented. Soil conditions investigated at two sites by way of undisturbed sampling using the ground freezing technique are described somewhat in details. The gravel-containing silty sand called Masado was identified to have developed liquefaction under intense shaking. The features of liquefaction and consequent lateral spreading which occurred in the reclaimed fills are presented in terms of attenuation characteristics of the lateral displacement of the ground diminishing with distance inland from the waterfront. As typical examples of the damage to foundations, results of in-site survey are presented on the injury of cast-in-place reinforced concrete piles of the bridge piers which were investigated by the pile integrity test and visual observation using the borehole camera. It was found that the major injury such as crack development had occur at the pile head, at the portion of soil stiffness discontinuity between liquefied and unliquefied layers, and also at the portion of discontinuity in stiffness of pile body. Outcome of comprehensive investigations on the damage to foundations of LPG storage tanks is described with emphasis of the behaviour of precast reinforced concrete piles. Lastly, simple analyses were made for the behaviour of piles undergoing lateral spreading. It was shown that, if piles were to move by an amount significantly larger than the surrounding soil deposit which was generally the case for the piles near the revetment lines, the stiffness of the soils must be reduced drastically when attempting to represent the soil-pile interaction behaviour by the spring model.

INTRODUCTION

The Hyogoken-Nambu earthquake, registering a magnitude of 7.2 (JMA), occurred before dawn at 5:47 am. on January 17, 1995 and delivered a very high level of devastating shock to densely populated area of Kobe-Osaka corridor which forms a major industrial heartland in the western part of Japan main island. The total death toll was over 6,000 and more than 300,000 people were left homeless. The very strong shaking collapsed approximately 150,000 houses and buildings, ignited fires, wrecked elevated highways and railways, and destroyed ports and harbour facilities. No less damaging was the loss emerging from business disruption and paralysis of industrial productivity resulting in a huge amount estimated to have been roughly 200 billion dollars worth, the highest record damage bill ever claimed by a single earthquake. Many strong motion records were obtained over the affected area. Peak ground acceleration as high as 0.83g and peak velocity as high as 175cm/sec were registered. These are the highest values ever obtained in terms of intensity and hence destructiveness of shaking. There is no doubt that such a high degree of shaking could be blamed for much of the havoc. There were a number of cases of destruction with geotechnical significance including slumping of revetment lines along the coast and periphery of the man-made islands, permanent settlements of the ground and failure of foundations due to liquefaction of the ground. The outcome of the in-situ and laboratory investigations conducted by various organizations will be described in the following pages of this lecture note.

SEISMICITY

Japanese archipelago is situated in a region where four major tectonic plates meet as indicated in Fig.1. It is well-known that major earthquakes have taken place in the historic time in the area of land upheaval due to subduction of the tectonic plates. As indicated in Fig.1 the Pacific Plate sinks towards the west, forming the Chishima trough. A series of seismic nests were created in the region of the upheaval west of the trough. Similar situations are encountered in the western edge of the Okhotsk Plate where Eurasia Plate subducts. The event associated with the crush of two crustal plates as above is known as "Inter-plate earthquake". In the eastern part of Japan, epicenters are generally located 50 - 150 km distant from the coast, but because of the events being fairly large in scale with a magnitude of the order of 8, effects of these earthquakes have been truly destructive.

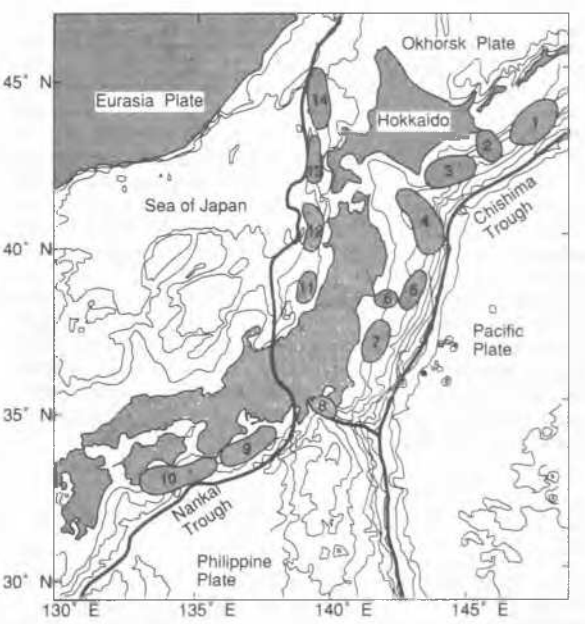

Fig.1 Tectonic plate-related seismic activities near the Japanese Archipelago

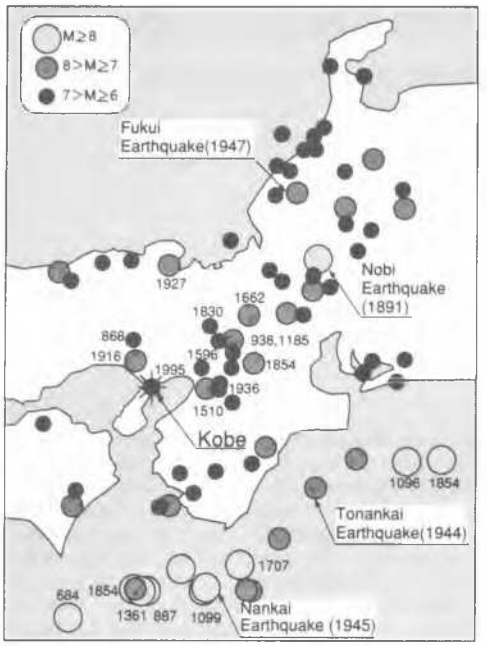

Fig. 2 Historical seismic activities in the Kansai region, Japan

Another type of earthquake occurred in Japan with an epicenter located in the region in-between two troughs which corresponds to the inland portion of the main island. This type of event is called "Intra-Plate earthquake". Because of its epicenters located underneath the land, intensity of shaking is very strong and their consequences are truly disastrous for local areas in their vicinity. The Kobe earthquake is identified as the intra-plate type earthquake, but because of proximity to the city, its effects were truly destructive in spite of its mediumly large magnitude being 7.2. Historically, a number of earthquakes are known to have hit the central part of Japan as shown in Fig.2. The largest ever event nearest Kobe was the Fushimi earthquake which occurred in 1596. Since then the area of Kobe has been seismically quiescent. Therefore, the quake in 1995 was unexpected and truly surprising.

SEISMIC GEOLOGY

The distribution of active faults in the area surrounding the Osaka Bay is displayed in Fig.3. While it is uncertain when each of these faults have been or will be activated, there are several of northeast to southwest oriented faults being disposed in echelon in the area of Rokko Mountains which are located north of the Osaka Bay. These in-echelon faults are considered to be caused by uplift of the land as a result of rupture of the earth crust. The mechanism of forming the Rokko Mountains accompanied by the fault rupture is envisaged by Fujita (1970) as illustrated in Fig.4. The large crustal force is postulated to act in the east-west direction as the major principal stress, and as observed in fracture of a rock specimen in the laboratory test, buldging takes place on the side of the minor principal stress. This bulge is interpreted as the same phenomenon as that encountered by the tectonic uplift of the land forming the Rokko Mountains.

GEOLOGY AND GEOMORPHOLOGY OF THE KOBE AREA

An overall feature of geological setting in the region of Osaka Bay is depicted in Fig 5. A cross section in northwest to southeast is shown in Fig.6 where it may be seen that sedimentary deposits of different geological eras exist in a bowl-shaped basin with a

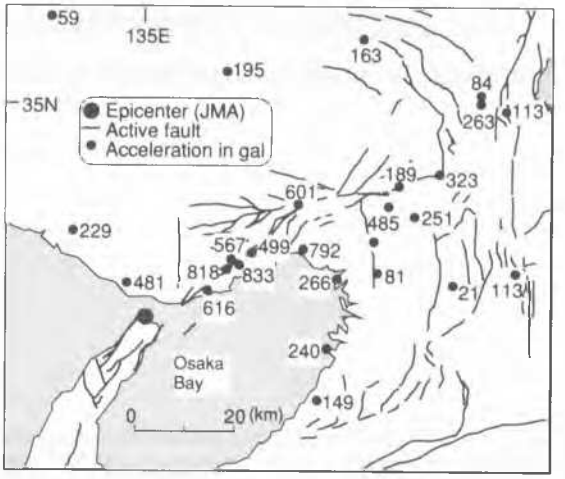

Fig.3 Distribution of fault ruptures in the bay area of Osaka

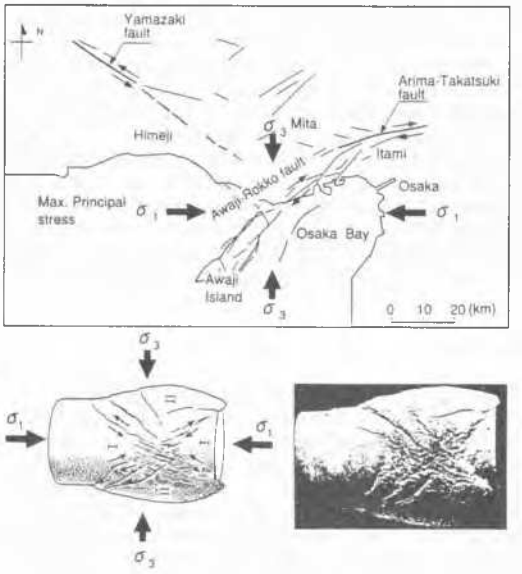

Fig.4 Illustration of the land upheaval and fault ruptures in Kobe area (Fujita, 1976)

maximum depth of about 2km. It can also be seen that there exist several offsets in the underlying rock formation indicating presence of fault rupture zones. They are considered to be sources of historical earthquakes in the long geological past. Kobe and its neighbouring cities such as Ashiya and Nishinomiya lie on the north-western side of Osaka Bay. As shown in Fig.7, they are located in the lowlands extending southwards from the foot of the Rokko Mountain Chain which consist of several fault blocks with steep escarpments towards the sea. The mountain areas with an elevation in excess of 300m are essentially composed of base rock such as granite and granodiorite. Formation of the lowland extending from the mountain to the coast is a consequence of water run-off which created a narrow flood belt and zones of numerous interconnecting alluvial fans as illustrated in Fig.7. Terrace deposits of Pleistocene origin are shown to exist in the area south of the Rokko Mountain. The Pleistocene deposits are overlain by Holocene alluvium composed of sand, gravel and clay which forms a relatively flat and narrow corridor of lands on which the city of Kobe developed. A cross sectional view in the cross section A-A' in Fig.7 is shown in Fig.8. It may be seen that several southward dipping layers of sand, gravel and clay do exist with overlying reclaimed fills near the surface. The clay-rich deposit under the man-made fills is the seabed sediment before the reclamation was conducted.

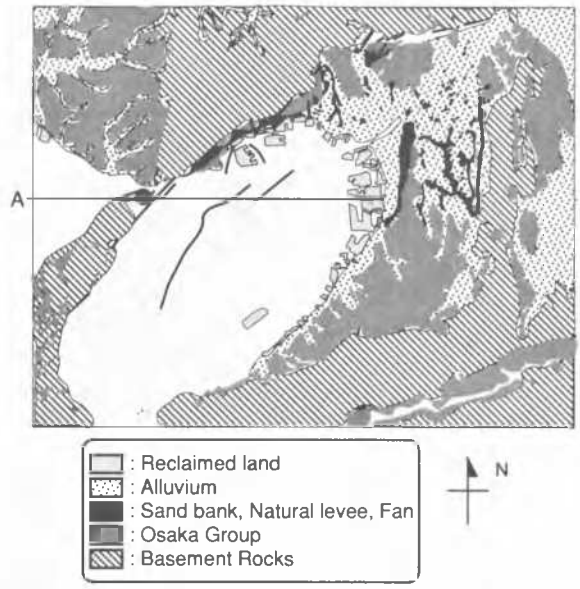

Fig 5 Geological map in the area surrounding the Osaka Bay

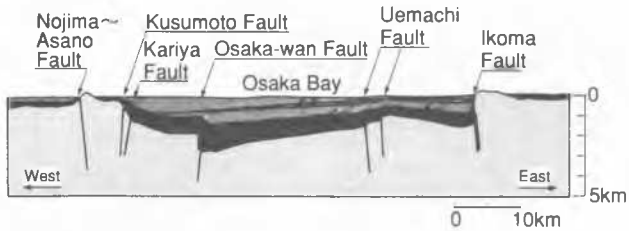

Fig.6 Cross sectional view of the geological regime in the Osaka Bay

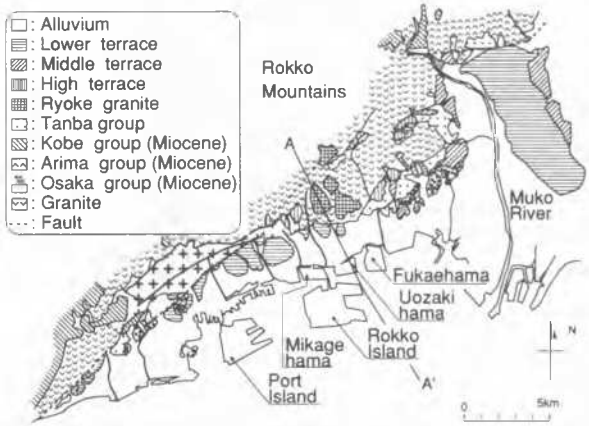

Fig.7 Geology and geomorphology in Kobe Bay area

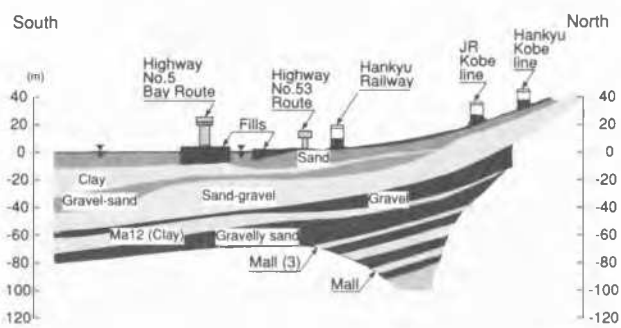

Fig.8 Subsurface soil profile in the Kobe area (Cross Section A-A' in Fig.7)

LAND RECLAMATION

Over the last two centuries a gradual but extensive reclamation of land has been underway along the bay margins of the Kobe district which is flanked by the Rokko Mountains. Several stages of land reclamation are described in Fig.9. In the era until 1959, the infilling was conducted in a relatively small scale along the natural shore line, but after 1960, a series of large-scale landfilling was performed off the shore. In the early period of reclamation work (Phase 1) in 1963 to 1970, eastern part of Kobe port was reclaimed to construct four islands, viz., Nada-hama, Mikage-hama, Uozaki-hama and Fukae-hama. Location of these islands is shown in Fig.10. The granite-derived soil materials were taken from borrow sites at the foothill of the Rokko Mountains located north of the reclaimed islands. In the second phase beginning in 1966, Port Island and northern portion of Rokko Island were constructed by transporting decomposed granitic soils from the borrow areas west of Kobe city. The borrow materials were transported to a nearby port by means of belt conveyors and brought to sites of landfilling by bottom-open push barges, as illustrated in Fig.10. Owing to the low strength and sensitivity of the soft alluvial clay in the sea bottom, the borrow soil was first dumped so as to spread uniformly to form a 2 to 3m layer, and then dumping was executed in steps to form each layer with a thickness of 3-4m. The barge dumping was continued until the fill reached an elevation about 2m below the water surface. Then, end dumping along the already constructed beach was performed above the water level. In the third phase the remaining part of the Rokko Island and the southern half of the Port Island were constructed by the materials composed of crushed

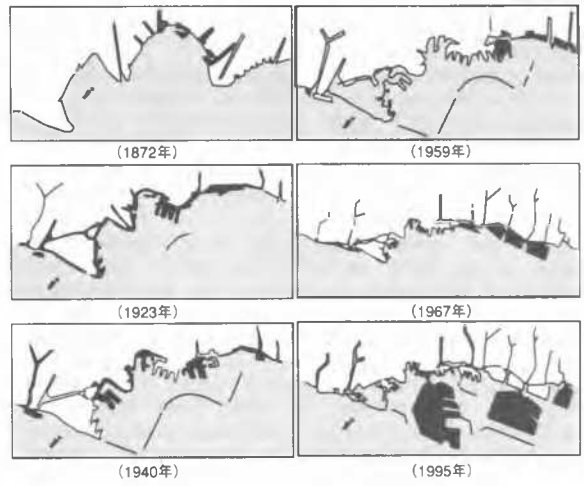

Fig.9 Development of land reclamation in the port district of Kobe

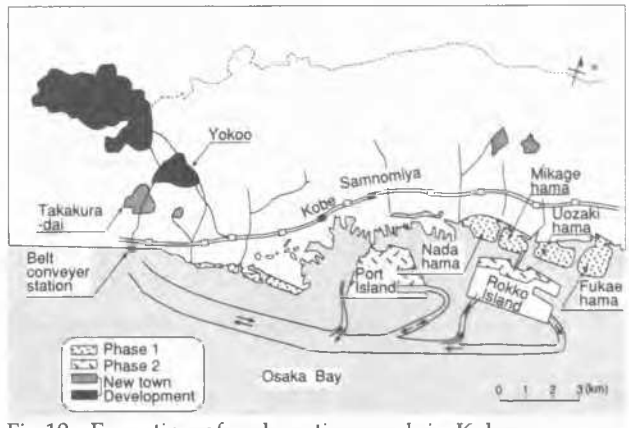

Fig.10 Execution of reclamation work in Kobe area since 1960's

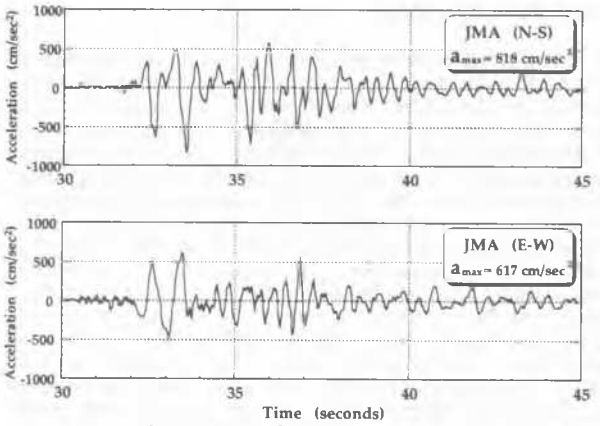

Fig.11 Time histories of horizontal acceleration recorded at Japanese Meteorological Agency

mudstone taken from the borrow area west of Kobe city. Thus, the ground in these areas consists of more silty soils with somewhat higher plasticity.

GROUND MOTION CHARACTERISTICS

At the time of the earthquake, a number of strong motion recording instruments were triggered and registered motions at various places in the epicentral region. One of the strongest motions recorded at the Japanese Meteorological Agency (JMA) is shown in Fig.11 where it can be seen that the peak horizontal acceleration on the ground surface was 818gal (83% of gravity acceleration) in the north-south direction. The peak velocity obtained by time integration yields a value as high as 175 cm/sec. The trajectory in plan of the recorded accelerations at JMA site is displayed in Fig. 12 along with other motions registered at sites in close proximity to the fault zone. The trajectories in Fig.12 reveal the fact that all of the seismic motions were predominantly oriented in the northwest-southeast direction which is perpendicular to the direction of fault line as indicated in Fig.13.

It is also known that the peak accelerations recorded in the hilly areas in the north are much stronger than the motions registered in the reclaimed deposits in the south where deamplication of the motions was significant due to nonlinear effects and also due to cyclic softening of soft soils prevailing in this area. On the basis of the recorded motions, it is possible to establish contour lines of equal peak horizontal acceleration as shown in Fig.13. It is seen that the oval-shaped contour lines are highly concentrated around the fault line indicating a rapid attenuation of the motions with increasing distance. To clarity this feature, the maximum recorded horizontal accelerations at various sites are plotted in Fig.14 against the distance counted from the nearest point on the fault line. It can be seen in Fig.14 that the shaking with the maximum accelerations of the orders of 500 to 800 gals occurred in the area within the distance of 5km from the fault line except for somewhat smaller accelerations recorded at sites of reclaimed deposits where liquefaction developed. Also noteworthy is the sharp attenuation of the motions in the area with the distance farther than about 20km. Typical relations of the same effect proposed by Joyner-Boore (1988) and Fukushima (1995) are also shown superimposed in Fig.14. These relations are considered to represent the attenuation characteristics of the seismic shaking during the Kobe earthquake with a reasonable degree of credibility.

The other recorded motions of supreme importance are those registered by the set of instruments which had been installed in a vertical array at a site in the northwest part of Port Island. Exact location of the instrument house is indicated in Fig.15. The soil profile at this site had been investigated to a depth of 84m as

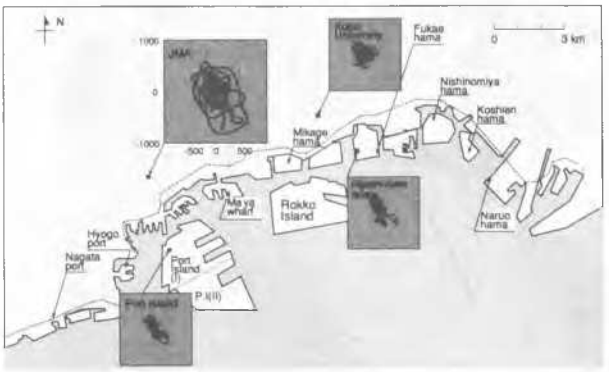

Fig.12 Trajectories in plan of horizontal accelerations recorded at four major sites

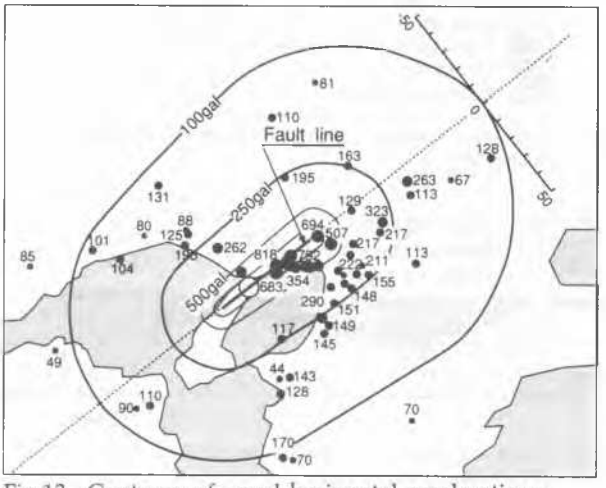

Fig.13 Contours of equal horizontal accelerations surrounding the fault line (Japanese Geotechnical Society, 1996)

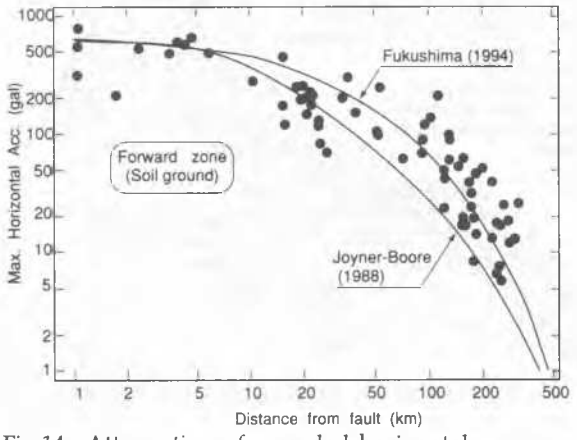

Fig.14 Attenuation of recorded horizontal accelerations in the Kobe earthquake (Japanese Geotechnical Society, 1996)

shown in Fig.16 where it may be seen that the reclaimed fills exist to a depth of 18m with SPT N-values of the order of 5 to 10. Beneath the reclaimed fills, there exists a silty clay layer which is identified as the seabed deposit before the reclamation.

Underlying this seabed deposit, there exist alternate layers of Pleistocene era composed of sands and silts occasionally containing gravel. Velocity logging was also conducted at this site to identify profile of shear wave velocity Vs and longitudinal wave velocity Vp. The results of these in-situ survey are displayed in Fig.16. The depths at which the strong motion recorders were installed are also indicated in Fig.16. The time

Fig.15 Location of sampling sites and vertical array site in Port Island

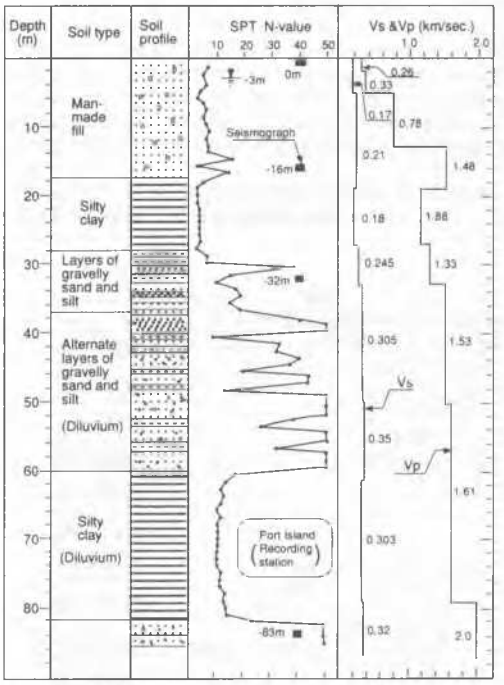

Fig.16 Soil profile at the site of vertical array of seismographs (Toki, 1995)

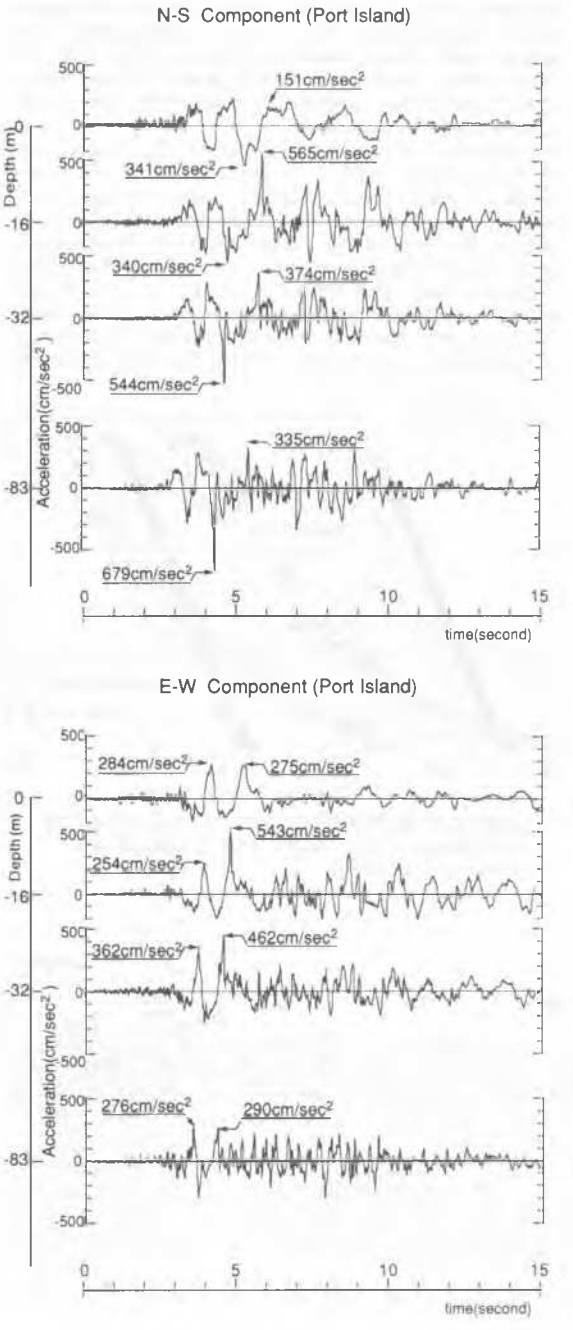

Fig.17 Horizontal accelerations recorded at the vertical array site of Port Island (Toki,1995)

histories of horizontal accelerations recorded at four depths are shown in Fig.17. In the case of north-south component, a peak acceleration of 679 gal at a depth of 83m is seen decreasing to a value of 544 gal at depth 32m, and further decrease to a value of 340 gal is observed to have occurred as the wave propagated upward to the ground surface. Similar deamplification is observed in the east-west component of registered acceleration for the near-surface deposit to a depth of 32m. It is apparent that cyclic softening of the reclaimed fills due to development of liquefaction could be the cause to account for such deamplification which would have otherwise been an amplification of the waves in the near-surface deposits. As indicated in Fig.12, the trajectory of this recorded motions at Port Island is oriented predominantly in the northwest to southeast direction. Thus the north-south component is to be taken as more representative of the motions that were encountered in the reclaimed deposits during the Kobe earthquake.

CHARACTERIZATION OF SOIL PROPERTIES

The fills beneath several island in the port area of Kobe were constructed using residual soil formed by weathering of granitic rocks. The soil dubbed Masado was obtained from borrow sites in the Rokko Mountain and brought to the site through a combination of conveyor belts and push-barges. This soil is collapsible in its natural state and its grain size distribution varies widely depending upon the degree of weathering. The general range of grain size for the decomposed granite fills are shown in Fig.18. The characteristic feature of the grain composition is that the material is generally well-graded and contains a significant fraction of gravel. Superimposed in Fig.18 are the ranges of gradation for soils which are highly likely or likely to develop liquefaction if the soils are deposited in-situ under sufficiently loose conditions. These ranges were established by examining the graduation curves of a

vast majority of soils which were known to have developed liquefaction in past earthquakes. In comparison with these boundary curves, the soils in Kobe area were known to have grain composition outside the boundaries and hence considered not to be highly susceptible to liquefaction.

To observe features of deposition in details, an attempt was made by Kobe city office (1996) to excavate an open pit in Ashiyahama Island assailed by extensive liquefaction. The location of the pit excavation is indicated in the map of Fig.19. As shown in a zoomed-up map in Fig.20, the site is just south of the No.5 Bay Route Expressway and known to have developed liquefaction as attested by spurting or oozing of sand-laden water at the time of the earthquake. In carrying out the excavation, a lot about 5m by 5m was enclosed by driving sheet piles and dewatering was performed while excavation was underway to a depth of 10m. The soil profiles around the four walls in the rectangular cross section were carefully canvassed and sketches drawn as shown in Fig.21. It may be seen that dumped materials composed of a potpourri of soils were deposited erratically and no clearly defined stratification is visible. Fig.22 shows one of the photographs taken at a depth of 10m. It may be seen that the soils derived from disintegrated granite were deposited without layered structures. The grain composition of the soils representative of those at each depth is shown on the right-hand side of Fig.21 where it can be seen that the gravel content is more than 50% throughout the depth at this pit location.

Following the earthquake, attempts were made by various agencies to recover high-quality undisturbed samples by means of the ground freezing technique. Shown in Fig.23 is the locations of these samplings. In all of the projects, the ground was frozen by circulating coolant through a tube placed in a borehole. As the freezing front was made to advance slowly in the radial direction, increased volume of pore water at the freezing front is considered to migrate outwards without disturbing intact structure of in-situ deposit. After freezing a column of in-situ soils about 1.5m in diameter, coring was performed to recover samples 15cm in diameter with a length of about 2m. The samples were wrapped with a vinyl sheet, transformed to the laboratory and stored in a frozer until they were tested.

Two sets of undisturbed sampling were carried out at two nearby sites; one at an uncompacted deposit and

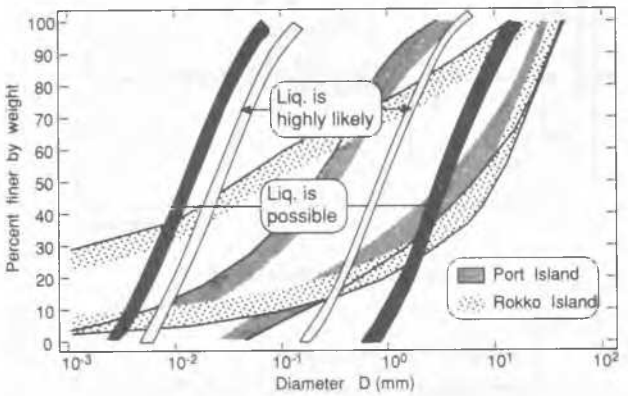

Fig.18 Grain size distribution curves of soils used for landfilling in Port Island and Rokko Island (Yasuda et al. 1995)

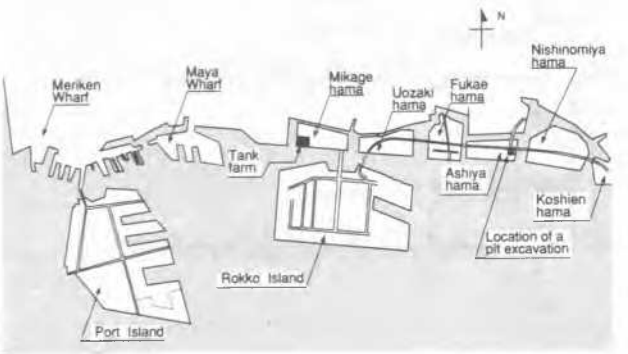

Fig.19 Location of pit excavation in Ashiyahama

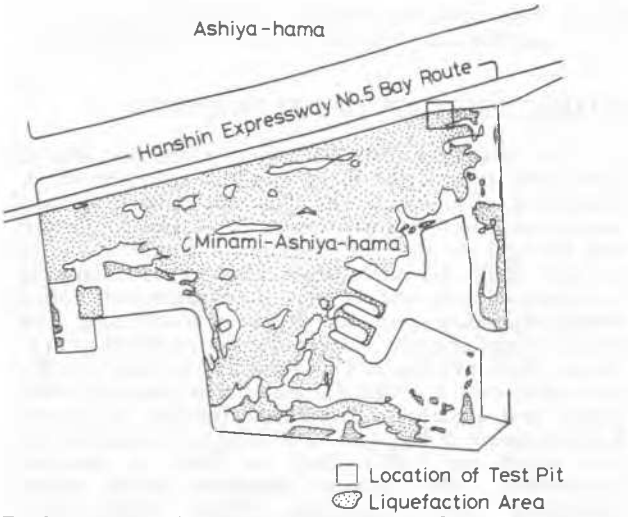

Fig.20 Feature of ground destruction in the vicinity of the pit excavation

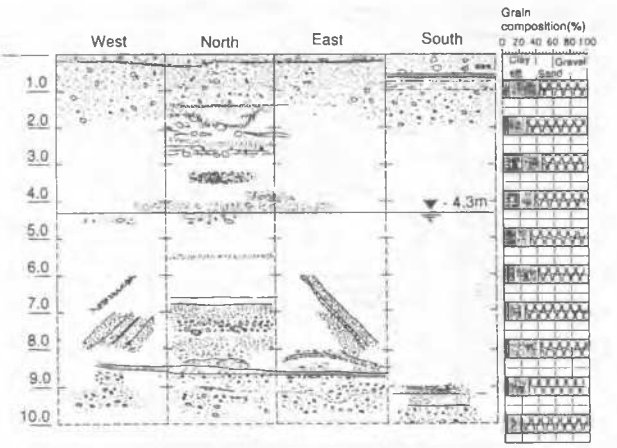

Fig. 21 Soil profile observed in the pit (Report of Hanshin Highway Authority, 1996)

Fig. 22 Soil profile at depth 10m at the site of excavation in Ashiyahama Island (Report of Hanshin Highway Authority, 1996)

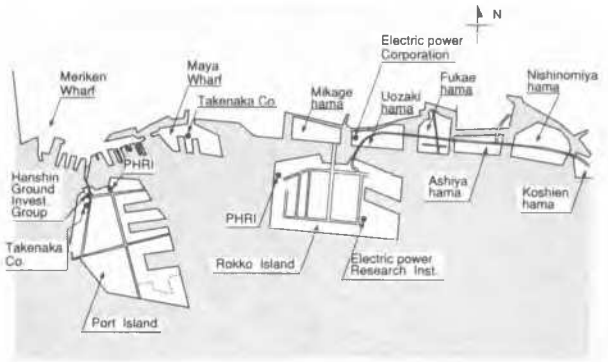

Fig. 23 Location of Sampling by means of the ground freezing technique

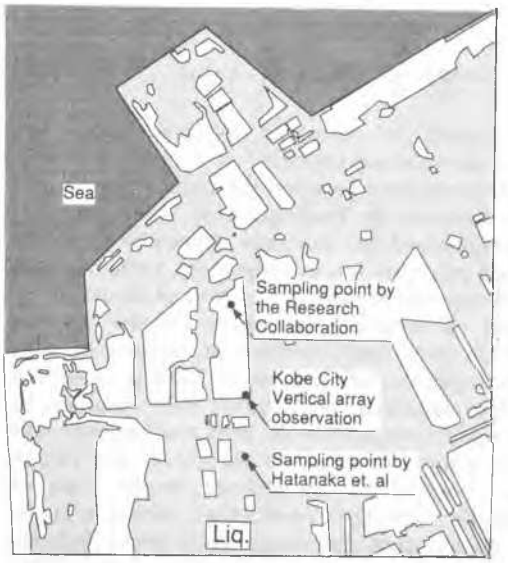

Fig.24 Features of liquefaction occurrence and location of sites of sampling and vertical array observation

the other at a compacted ground in the northern part of Port Island as indicated in Fig.23. Somewhat zoom-up map shown in Fig.24 indicates that the two sampling sites are in the vicinity of the vertical array observation site and apart only within a distance of 250m.

At one site where sampling was performed by Hatanaka et al. (1996), evidences of liquefaction such as sand boiling and ground rupturing were observed all over the surface. At the other site where sampling was conducted on the compacted deposit by the Research Collaboration team (Geotechnical Research Collaboration, 1997), surface manifestation of liquefaction was not witnessed following the earthquake. Thus it would be of interest to compare results of in-situ and laboratory tests conducted on the soils at these two sites.

At the compacted site, the reclaimed deposit had been densified by means of what might be called "Rod compaction method" in which a H-shaped steel beam 40cm by 40cm was driven into the ground while vibrating vertically. The space formed in the beam cross section during penetration was filled with sand which was supplied from the ground surface. As a result of this operation, a column of densified sand about 60cm in diameter was created resulting in the compaction of loose sand deposits in its neighbourhood. The compaction had been performed to a depth of 18m in the area where warehouses for packing were to be constructed, as shown in Fig.25. The results of in-situ sounding tests by means of the Standard Penetration Test (SPT) are displayed in Fig.26. Although there are scatters, the SPT N-values for the compacted deposits are known to be in the range of N=15 to 45 with an

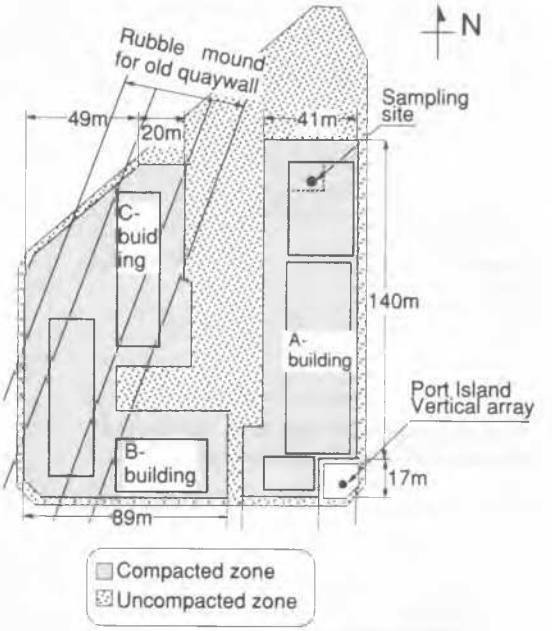

Fig.25 Plan view of the packing house site

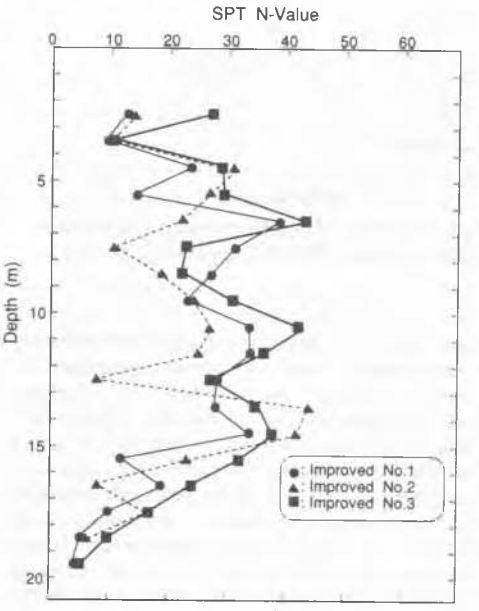

Fig.26 SPT N-values at the site of the packing house

average of about 30. It is to be noted that the near-surface layer shallower than 5m and the deep-seated layer deeper than 15m had not be densified enough. Presence of more fines in the deep layer and lack of enough surcharge near the surface are believed to be the reasons for the incomplete compaction there evaluated in term of SPT N-value.

The undisturbed frozen samples cut so as to have a diameter of 15cm and 30cm in length were once thawed and tested in the laboratory using the cyclic triaxial test apparatus. The results of the cyclic triaxial tests on samples recovered from depths 5.8 - 6.7m are shown in Fig.27. The samples contain about 50% gravel (particle size greater than 2mm) as shown in the grain size distribution curves of Fig.28. Fig.27 indicates that the cyclic shear strength defined as the cyclic stress ratio causing 5% double-amplitude (D.A.) axial strain in 20 cycles of uniform load application is of the order of 0.25 - 0.35, which is apparently greater than that normally obtained for samples of loosely deposited clean sand. It is noted that, unlike the behaviour of other undisturbed

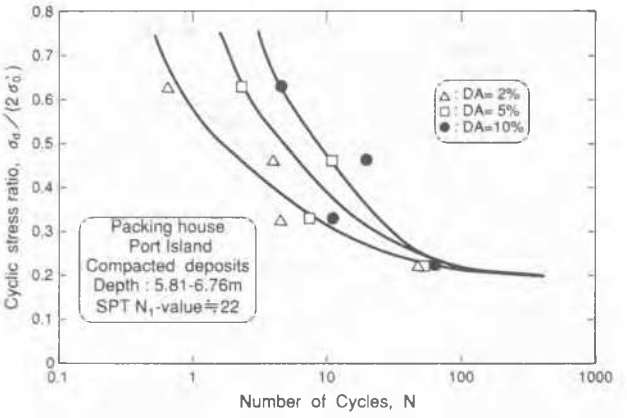

Fig.27 Cyclic strengths of soils from compacted deposit at the packing house site

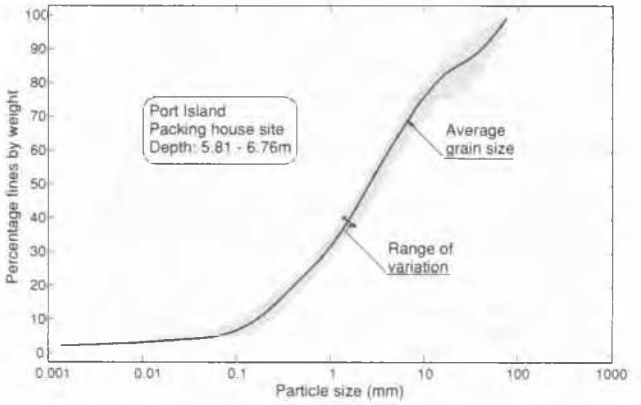

Fig.28 Grain size distribution of the Masado soil from the depth of around 6m at the packing house site

samples of clean sand, the cyclic strength has tendency to increase significantly with decreasing number of cycles. The cyclic strength as defined for various numbers of load application, Nc, is plotted versus SPT N_1 – value in Fig.29, where N_1-value is the SPT N-value normalized to that undergoing a confining stress of 1kgf/ cm^2. It is apparent that the cyclic strength tends to increase with increasing N_1-value and also with decreasing number of cyclic load application being considered. The rise in cyclic strength is observed to be more pronounced as the number of cycles in question becomes smaller.

Another scheme of sampling by means of the ground freezing was conducted by Hatanaka et. al. (1997) at an uncompacted site in close proximity to the packing house site as mentioned above. Exact location of the sampling is shown in Fig.24. The soil profile at this as-deposited site is presented in Fig.30 where it can be seen that a uniform layer of the granite-derived Masado exists to a depth of 18m with an average SPT N_1 – value of 10. The outcome of the cyclic triaxial tests on undisturbed samples from this site is displayed in Fig.31 where it can be seen that the cyclic strength for 20 cycles and 3 cycles is 0.18 and 0.30, respectively, on the average. Grading of the tested materials is shown in Fig.32. The values of the cyclic strength obtained from this test series are also presented in Fig.29 in term of the plot against SPT N_1 – value, along with the data from the compacted site. Comparison of these two data sets, one from the compacted and the other from the uncompacted deposits, clearly shows increases in cyclic strength as well as N_1 – value for the samples from the

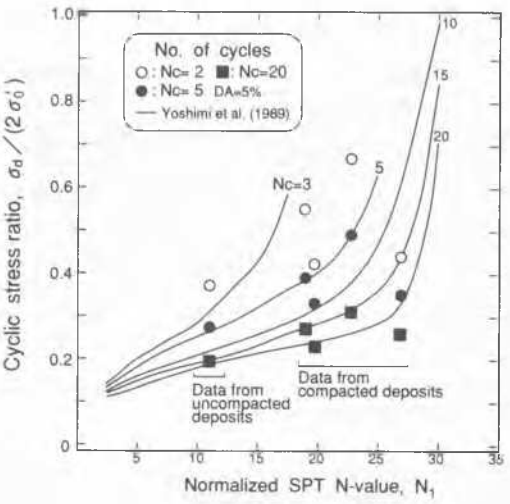

Fig.29 Cyclic strength versus N_1 – value

densified deposit, as compared to those from the undensified as-reclaimed deposit.

In Fig.29, relations between the cyclic strength and N_1 – value proposed by Yoshimi et al. (1989) are also shown superimposed by solid lines. It may be seen that the proposed relations are in agreement with the data described above with a reasonable degree of accuracy.

Projects of sampling by means of the ground freezing have been implemented at dozens of sites throughout Japan including those in Kobe area shown in Fig.23. The wealth of high-quality data obtained by the cyclic triaxial tests and in-situ tests was amassed and compiled in a form of empirical formulae, and put in the revised version of the seismic design code of Japanese Highway Bridge Construction. Shown in Fig.33 is a curve quoted from this design code which belongs to sandy soils having fines content less than 10%. Individual points in this figure are those of test data from the laboratory tests on undisturbed samples. In fact, the design curve shown in the figure was established based on these data. The curve in Fig.33 indicates that the cyclic strength of sandy soils starts to increase remarkably for the range of N_1 – value in excess of 20. It may also be seen that the upper limit of N_1 – value beyond which liquefaction-type cyclic softening never occurs is about 30.

LATERAL SPREADING OF THE GROUND

During the earthquake, liquefaction developed extensively over the areas of reclaimed lands in the port and harbour district of Kobe city. In the terrain behind the quaywalls, the liquefaction gave rise to an increase in lateral force, and led to excessive movements of the caisson-type wall as much as 3 to 4m towards the sea. A certain percentage of this movements may be attributed to a pure translation of the wall caused by the inertial force due to very high intensity of ground shaking during the earthquake. Whatever the genetic cause is, the horizontal movement of the wall was accompanied by an equally large amount of lateral spreading of ground soils which propagated rearwards inland. The ground rupture as it propagates backwards is to be considered as a phenomenon of engineering significance as it defines the spatial extent of the ground distress to which due consideration may need to be given in relation to the design of foundations, in order to allow for the effects of lateral spreading. In view of this, attempts were made to investigate features of ground displacements and settlements caused by the lateral spreading of liquefied soil during the earthquake

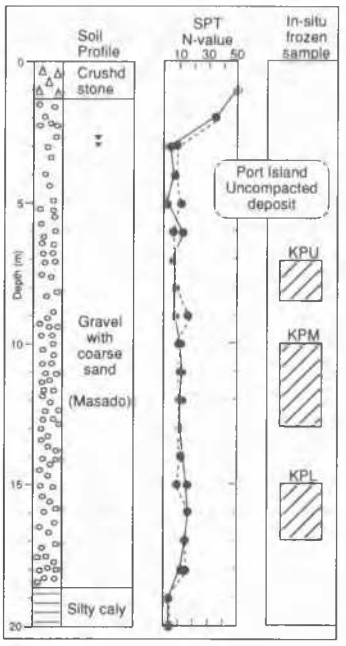

Fig.30 Soil profile at the uncompacted site in Port Island (Hatanaka et al. 1997)

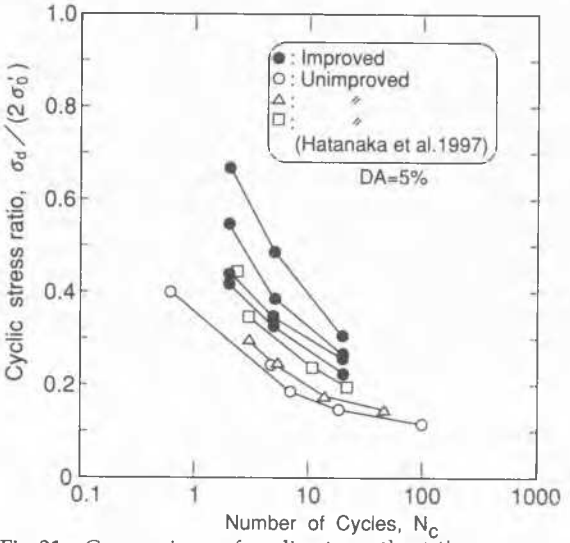

Fig.31 Comparison of cyclic strength of the undisturbed samples from uncompacted and compacted Masado deposit

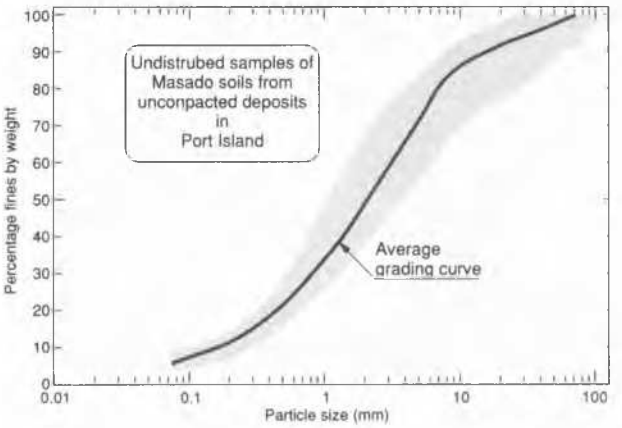

Fig.32 Grading of the undisturbed samples of the Masado soil from the uncompacted site (Hatanaka et al. 1997)

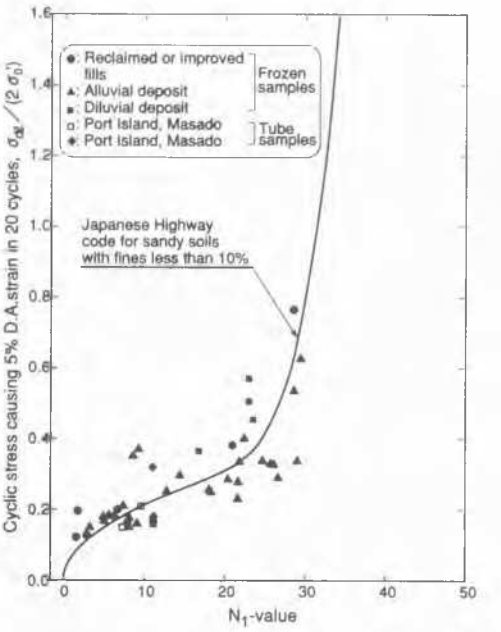

Fig.33 Cyclic shear strength versus SPT N_1-value

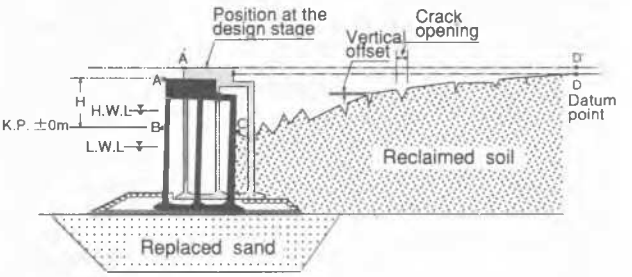

Fig.34 Schematic diagram illustrating items of measurements in the method of the ground surveying

in the wharf areas along the peripheries of Port Island, Rokko Island and Fukae Island. At a number of locations, measurements were made on the width of open cracks and vertical offsets across the cracks on the ground surface along an alignment in the direction perpendicular to the revetment line. The scheme of survey on the ground surface is illustrated in Fig.34. The in-situ measurements started from a point C behind a quaywall until a datum point D is reached where there is no crack visible on the ground surface. By summing up the width of the crack openings successively from the datum point towards the waterfront, the lateral displacement at any place was determined. Similarly by summing up the vertical offsets, the distribution of settlements was obtained as a function of distance inland from the waterfront where caisson-type quaywalls are installed. The locations where measurements were made are shown in Fig.35. They are all located in the peripheries of man-made reclaimed islands consisting of practically the same materials, i.e., Masado derived from weathering of granitic rocks. The revetments or quaywalls in this area were all constructed of gravity-type caisson walls with their inner compartments filled with sand. A vast majority of the caisson boxes were placed on the stone mounds resting on the Masado beds, which were artificially placed after the soft clay in the original seabed was removed. The material behind the caisson walls is also the Masado, the same soil as used for the foundation bed. A typical result of measurements is displayed in Fig.36 for the cross section R-2 in Rokko Island where it can be seen that the caisson body did stoop, accompanied by a lateral movement of 1.56m and

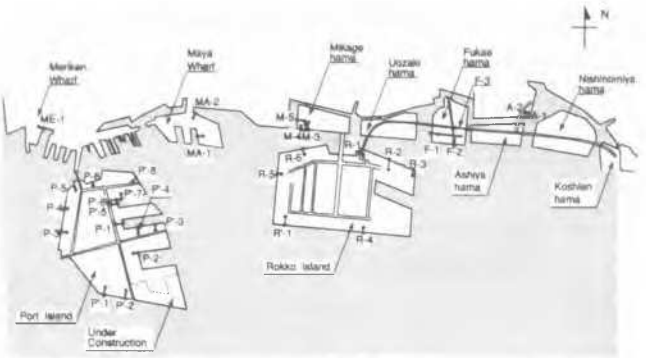

Fig.35 Location of cross sections where measurements were made using the ground survey method

settlement of 0.96m. The displacement is shown to have extended inland as far backwards as 183.7m. A soil profile near the point R-2 is shown in Fig.37. It may be seen that the man-made fills composed of Masado soil existed to a depth of about 20m. Liquefaction is conceived to have occurred in this reclaimed fills. It is conceivable that there were dual factors which might have acted to produce the lateral displacement of the caisson walls. These are inertia force due to the intense shaking and softening of soils surrounding the caisson caused by buildup of pore water pressure. It may be roughly assumed that the effects of pore water pressure buildup including liquefaction were, by and large, the same all over the waterfront areas in Kobe port that were affected by the earthquake. However, the effects of inertia force are deemed different, depending upon the direction to which the revetment line is oriented. As a matter of fact, the records of accelerations secured during the earthquake showed motion characteristics which are largely biased to the northwest-southeast direction as indicated in Fig.12. Based on the records obtained nearby, the acceleration inferred to have acted on the quaywalls oriented in different directions were established by Inagaki et al. (1996) as indicated in Fig.38. It may be seen that the horizontal acceleration against the north- or south-facing walls was of order of 500gal whereas an acceleration of the order of 250-300gal is inferred to have acted against the east- or west-facing walls. Reflecting such directionality of the earthquake motions, the lateral displacements at the caisson points obtained by GPS (Inagaki et al. 1996) were of the order of 2-4m in the north- or south-facing walls, which were apparently larger as compared to the value of 1-3m in the walls facing the east or west, as shown in Fig.39.

In view of this, all the data on the ground displacements measured by the method of the ground surveying at Port Island, Rokko Island and Fukaehama were divided into two groups; one pertaining to the north- or south-facing walls and the others to the east- or west-facing walls. Fig.40 shows all the lateral displacements from the north- or south-facing caisson walls plotted together, versus the distance from the line of revetment. It is noteworthy that there is an acute drop in the displacement in the vicinity of the walls, which is indicative of pronounced influence of inertia force in producing the large displacement near the walls. Fig.41 shows all the data of the ground displacement obtained at the sites where the quaywalls are oriented towards the east or west. As compared to similar data arrangements shown in Fig.40, the attenuation of lateral displacement is seen in Fig.41 being more gradual even in the are a in proximity to the walls. The lateral displacement at any point normalized to that at the waterfront is shown in Fig. 42 for the east or west facing walls against the distance which was also normalized to the maximum distance within which the ground distorsion such as cracks was observed. Similar data arrangements were made also for the north or south facing walls. Though there are scatters in the attenuation curves, it may be possible to draw an average curve as indicated in Fig.42. The average line drawn in Fig.42 is displayed again in Fig.43, along with similarly obtained average curve for the north or south facing walls. It can be seen in Fig.43 that the attenuation is more pronounced for the soil deposit retained by the north- or south-facing caisson walls than for the ground behind the walls facing the east or west direction. The reason for the rapid attenuation in the former case is simply the larger movements of the quaywalls which were caused by a greater acceleration in the north-south direction during the Kobe earthquake. As discussed above, the ground movements in the backland retained by the east- or west-facing walls appear to have been

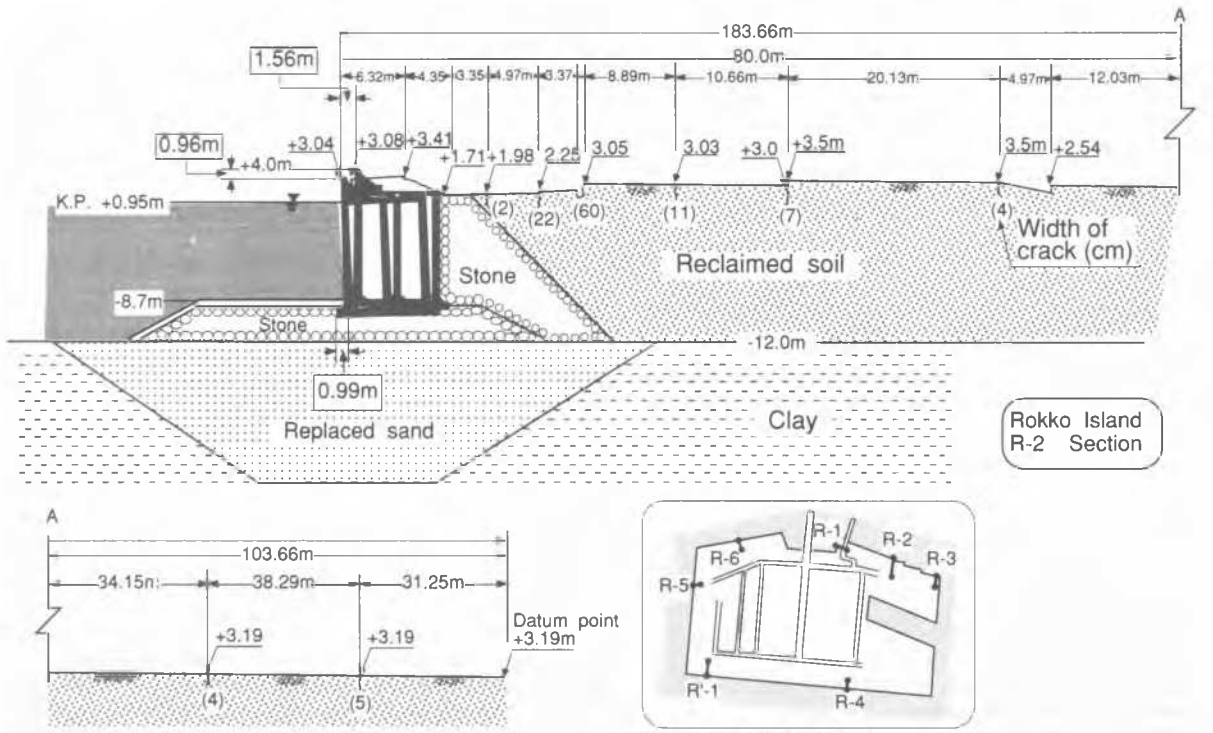

Fig. 36 Detailed profile of the ground deformation at R-2 Section in Rokko Island

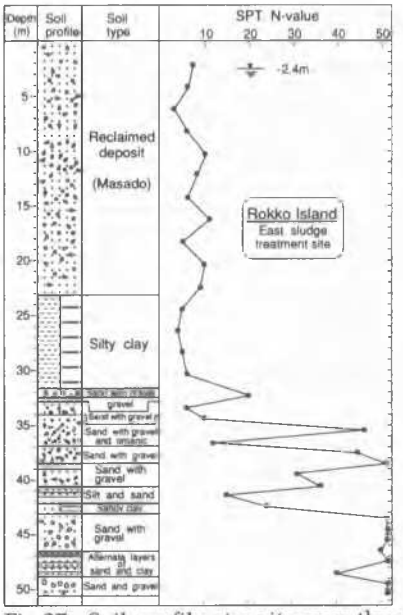

Fig.37 Soil profile at a site near the section R-2 and R-3 (Hanshin Highway Authority, 1993)

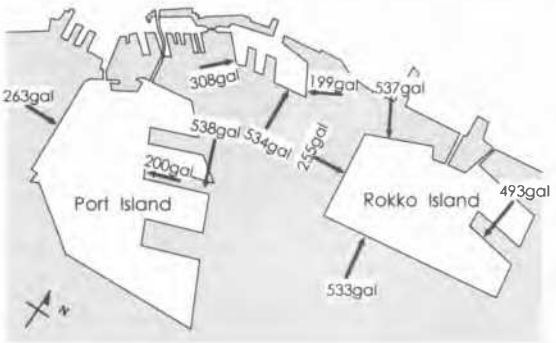

Fig. 38 Magnitude of acceleration inferred to have acted on the quaywall with different directions (Inagaki et al., 1996)

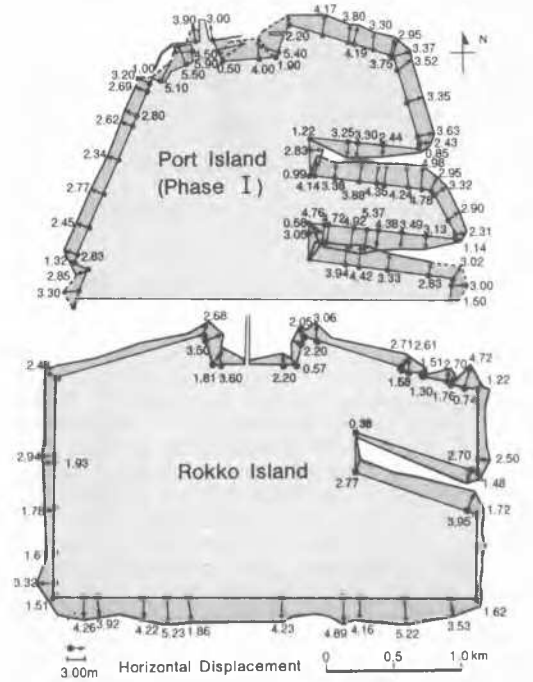

Fig.39 Lateral displacements of the quaywalls in Rokko Island and Port Island (Inagaki et al., 1996)

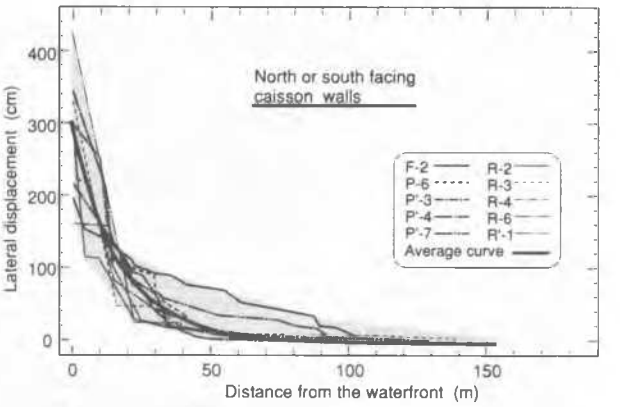

Fig.40 Lateral displacements versus the distance from the waterfront (North or south facing quaywalls)

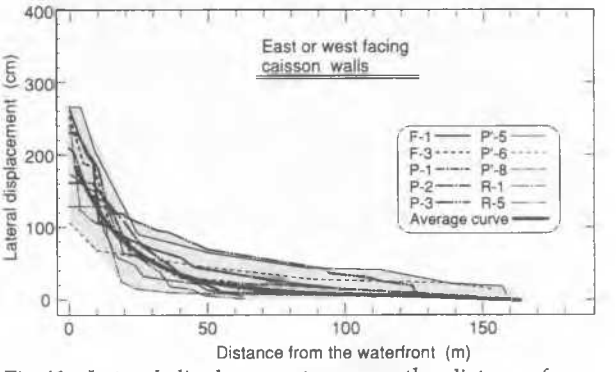

Fig.41 Lateral displacements versus the distance from the waterfront (East or west facing quaywalls)

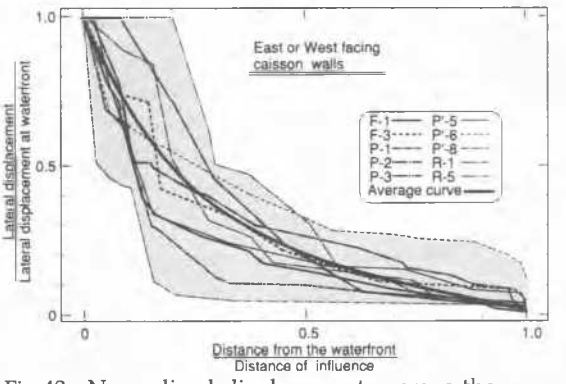

Fig.42 Normalized displacements versus the normalized distance from the waterfront (East or west facing quaywalls)

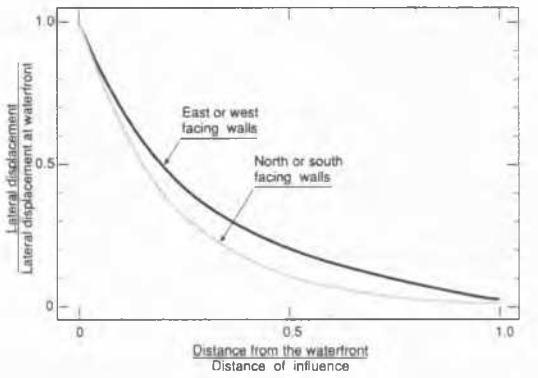

Fig 43 Comparison of the normalized displacement versus the normalized distance for the quaywalls with different directions

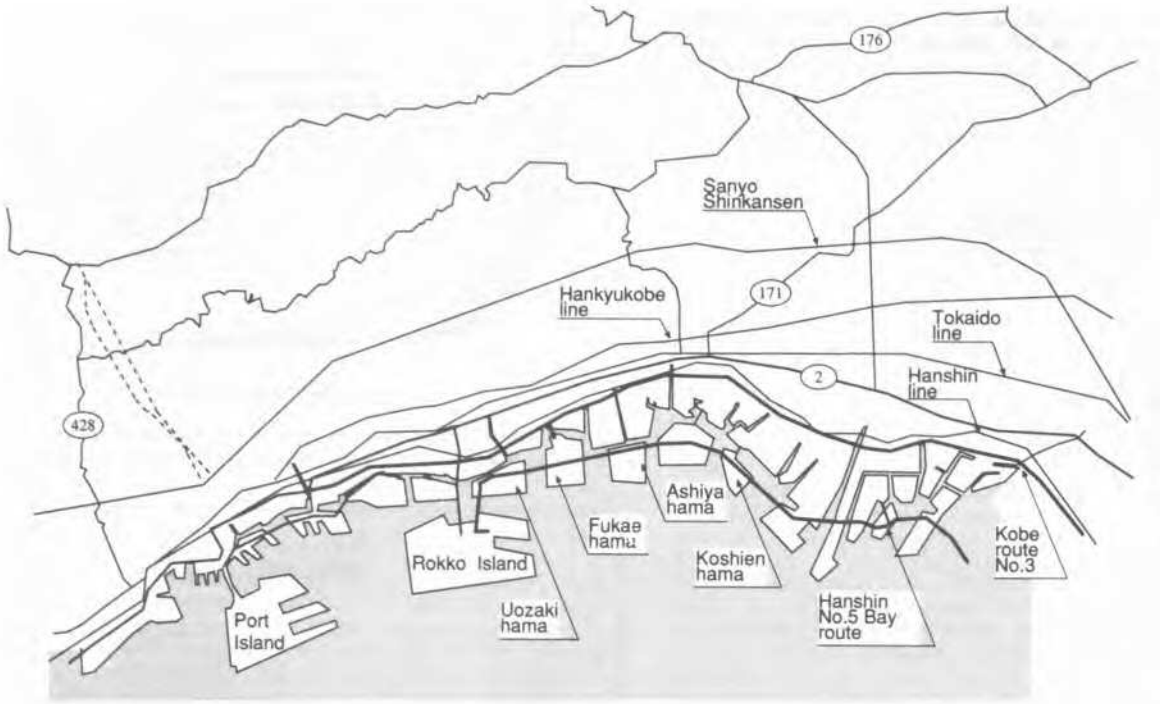

Fig.44 Highway system in the Osaka-Kobe district

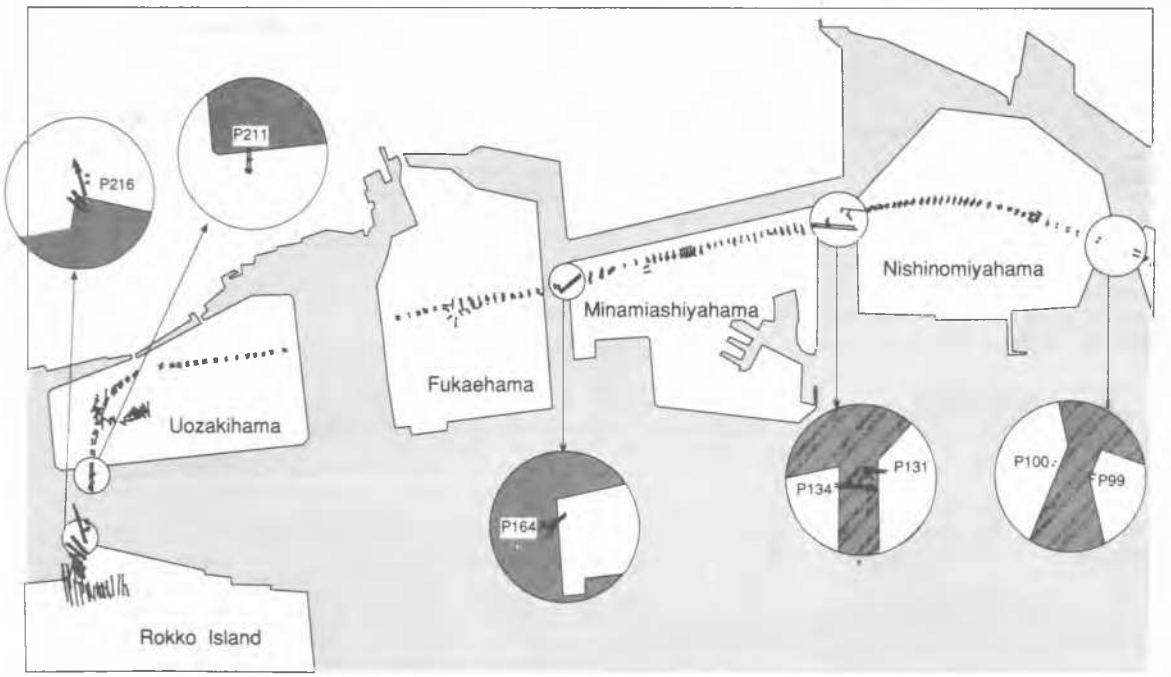

Fig.45 Lateral displacements of the bridge piers along the No.5 Bay Shore Highways (Hanshin Highway Authority, 1996)

caused primarily by the liquefaction of the soil deposit, and for this reason, it would be legitimate to choose the attenuation curve pertaining to the east- or west-facing walls for practical purposes where estimate of lateral displacements is needed considering the ground shaking of the order of 300gal, for design of foundations or underground structures.

DAMAGE TO BRIDGE FOUNDATIONS

Extensive damage was incurred to water-crossing bridges and elevated structures of the Hanshin Expressway along the bay area between Kobe and Osaka. This is a network of major toll highways and interlining feeder routes constituting one of the primary arterial highways within this region. Fig.44 shows the network of the expressway in the heavily damaged area of the Hanshin (Osaka-Kobe) district. The highways most fatally affected were No.3 Kobe Route and the No.5 Bay Route. The Route No.3 is a major toll highway extending from Osaka, alongside Osaka Bay through to the western side of Kobe and is almost entirely elevated throughout the route. The main feature of the damage was the breakage of reinforced concrete single pillars due to excessive shear stress or bending moment induced by strong inertia force during the intense shaking of the Kobe earthquake. It is reported by Iwasaki (1996) and Matsui et al. (1996) that the damage to elevated structures for the No.3 Kobe Route were concentrated mainly to the piers above the ground supporting the superstructures and little

damage was incurred to the foundations such as embedded footings and piles.

In the case of the No.5 Bay Route, the damage to piers or superstructures were more than severe in the terrain close to the waterfront. No less destructive was the damage to foundation system such as piers or footings. The Bay Route is located in the area of manmade deposits composed of the Masado soil in Kobe. Following the earthquake, movements of bridge piers were surveyed along the Bay Route No.5 by virtue of the GPS (Global Positioning System). The outcome of the survey is displayed in Fig.45 in terms of vectors for the section from Nishinomiya to Rokko Island. It was discovered that the vast expanse of the area surveyed had moved as a whole about 20cm towards southwest for some reasons not yet identified. In the displacement vectors displayed in Fig.45, the overall movements of 20cm are subtracted from the measured data. Fig.45 indicates that the lateral displacements of the bridge piers in the vicinity of the waterline are generally larger than those in the inland area and directed predominantly towards the waterfront.

The ground displacements in some sections along the Bay Route No.5 were estimated by Hamada et al. (1996) over the widespread area by means of air-photograph interpretation. In this method, some target objects on the ground such as manholes or corners of drainage channels were pinpointed and designated on pairs of air-photographs taken before and after the earthquake and the displacements were obtained by taking the difference between the post-and pre-earthquake locations of these objects. The lateral displacements obtained in this way at specified points were used to obtain a picture of distribution of the horizontal displacements, based on a linear interpolation method using a finite element mesh. The picture of lateral displacements thus obtained for the southern part of Uozakihama is displayed in Fig.46, where it may be seen that in the area near the revetment line the lateral displacement is directed southwards to the waterfront with its maximum of 186cm. Note that the lateral displacement of the bridge pier, P211, closest to the revetment was 62cm a value which is significantly smaller than that of the surrounding ground.

The most striking feature of the damage was movement of foundations towards the sea due to lateral spreading of the ground as a whole resulting from liquefaction of soils. Deleterious effects of lateral spreading were notably observed in performances of piers or bents of elevated highway structures standing in proximity to revetment lines. A typical example of such damage was seen in the Pier 211 of the Hanshin Expressway No.5 Bay Route which is located in the southernmost part of Uozakihama Island as shown in Fig.46. Features of the ground damage in the vicinity of Pier 211 are displayed in Fig.47 together with a plan view of the pier. Several lines of fissures are visible on the ground surface near the revetment. Somewhat

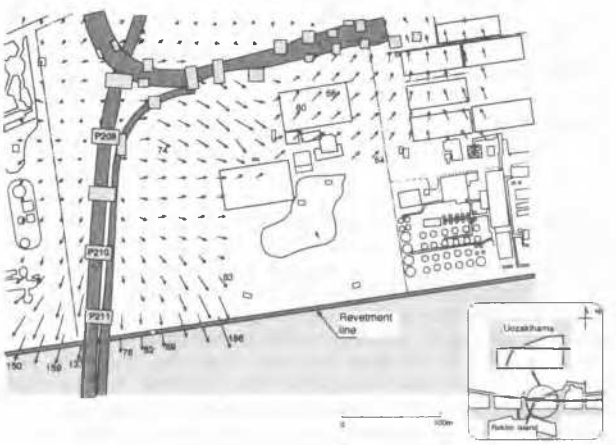

Fig.46 Ground displacements in the south part of Uozakihama Island
(Hanshin Highway Authority, 1996)

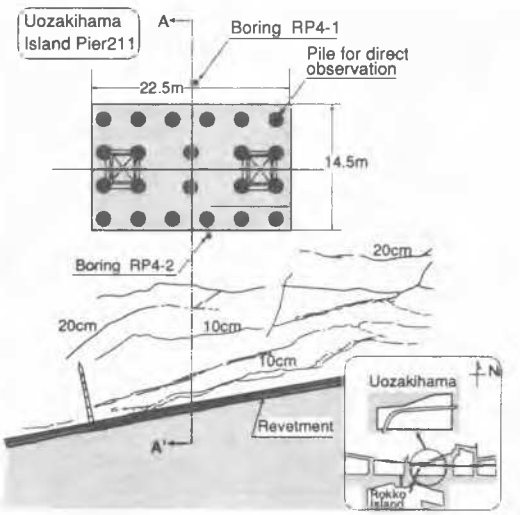

Fig.47 Ground distorsion and location of Pier 211
(Hanshin Highway Authority, 1996)

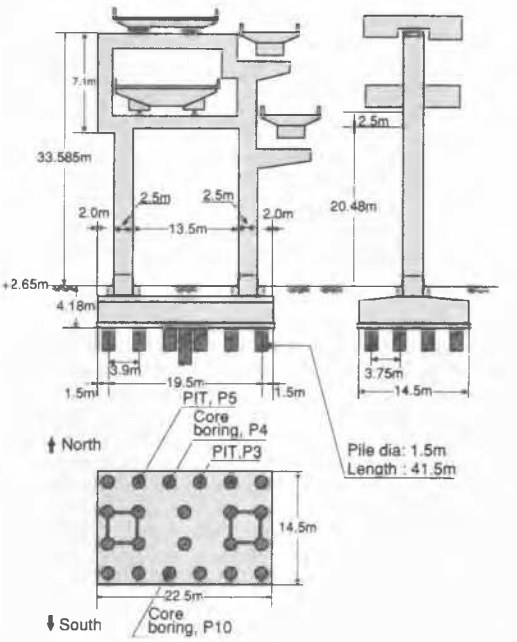

Fig.48 Plan and side views of Pier 211
(Hanshin Highway Authority, 1996)

enlarged plan view of the foundation is shown in Fig.48 where it can be seen that two-column bents sit on a 22.5m long and 14.5m wide footing which is supported by 20 piles 1.5m in diameter. The piles were constructed of cast-in-place reinforced concrete. Side views of the Pier 211 are shown in Fig.48 where it is noted that the body of the footing is embedded to a depth of 4.18m. A cross sectional view of the foundation and the quaywall across the section A-A' in Fig.47 is displayed in Fig.49, together with a soil profile. Exact location of the soil profile investigation (RP4-1) behind the quaywall is shown in Fig.47. As a result of measurements by GPS, it was discovered that the Pier 211 had moved towards the sea by 62cm, as accordingly indicated in Fig.49. It is highly likely that liquefaction developed in the reclaimed fills in the backland leading to widespread occurrence of lateral spreading as demonstrated in Fig.46. The lateral displacement of the ground in close proximity to the Pier 211 but free from its influence, may be read off from Fig.46 as being of the order of 100cm.

To investigate the damage feature incurred to the foundations, three methods were employed for the bridge piers along the No.5 Bay Route line: (1)

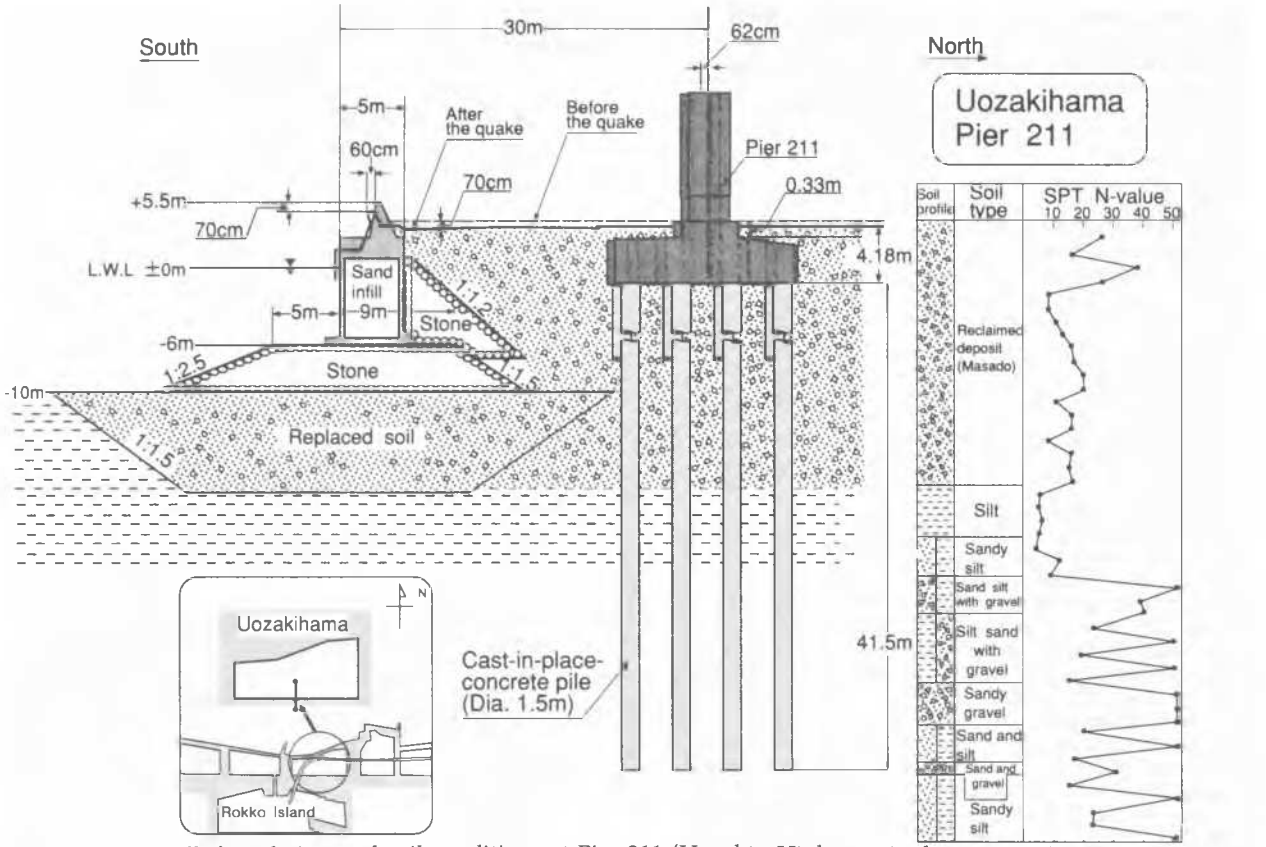

Fig.49 Quaywall, foundation and soil conditions at Pier 211 (Hanshin Highway Authority, 1996)

excavation to the level of the pile head below the bottom of footings; (2) picture-taking by means of video camera lowered to bored holes and (3) non-destructive method called "pile integrity test" using transmission of reflected waves. For the investigation of piles supporting Pier 211, excavation was executed to a depth of 6m at the northeast corner of the footing, as shown in Fig.50, by enclosing a 3.2m by 4.5m section using sheet piles. More detailed side and plan views are shown in Fig.51. Visual observation at the pile head disclosed several vertical and horizontal cracks a few millimeters wide as shown in a photograph in Fig.52. In the second method of in-situ investigation, a bore hole 7cm in diameter were drilled by the method of coring from the top surface through the footing slab down into the pile, as illustrated in Fig.53. If it happened to hit the reinforcement midway, another hole was drilled to reach a desired depth of 34m. A total of 2 holes were drilled to a depth of 34m for the inspection of damage in the foundation of Pier211. Exact locations of the holes are shown in Fig.48. A video camera was lowered into the holes to examine feature of cracking around the walls. Typical examples of video camera image at depth 0 -2.0m and 21.0 - 23.0m are displayed in Fig.54 where it is observed that several cracks developed down to a depth of 1.0m from the head of the pile P4 in Pier211. Cracks were also detected at various depths as represented by those at a depth of 22.0 - 23.0m shown in Fig.54. By and large, cracks were predominantly observed at depths corresponding to the boundary in soil deposits where liquefaction did and did not developed.

As a convenient technique of in-situ survey, the pile integrity tests were carried out at a number of piers along the No.5 Bay Route. The principle of this test is illustrated in Fig.55. Compressional waves produced by hammer hitting on the footing surface propagate downwards through the pile. Upon encountering an irregularity such as cracking, a reflected wave is generated coming back to the surface some instants afterwards. By detecting the length of time required for the reflected wave to reach the surface, it becomes

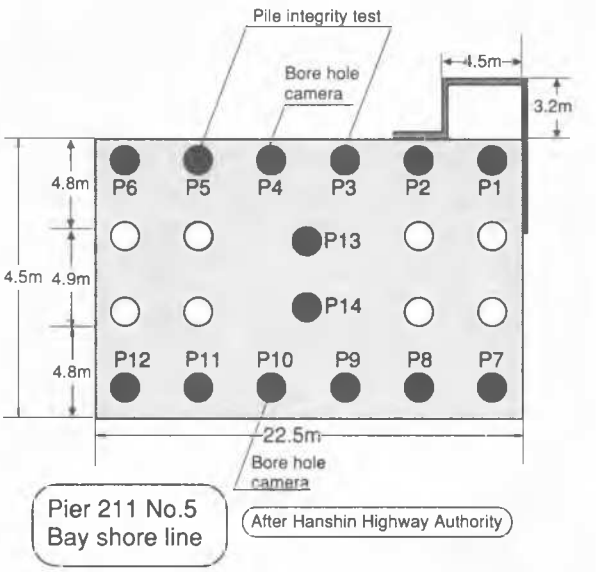

Fig.50 Plan view of the foundation of Pier 211 (Hanshin Highway Authority, 1996)

possible to identify a location of the crack for a known velocity of wave propagation through a concrete pile. The results of the pile integrity tests are expressed in terms of the number of cracks detected per 2m length of a pile. The results of this counting at piles P3 and P5 is displayed in Fig.56 together with a soil profile at RP4-2 shown in Fig.49. It may be seen that the number of cracks is concentrated near the pile top just below the footing slab where the bending moment is supposed to have been the greatest during the back and forth movement of the piles in the main shaking of the earthquake. Note that the pile top was rigidly plugged into the slab and therefore fixed connection was

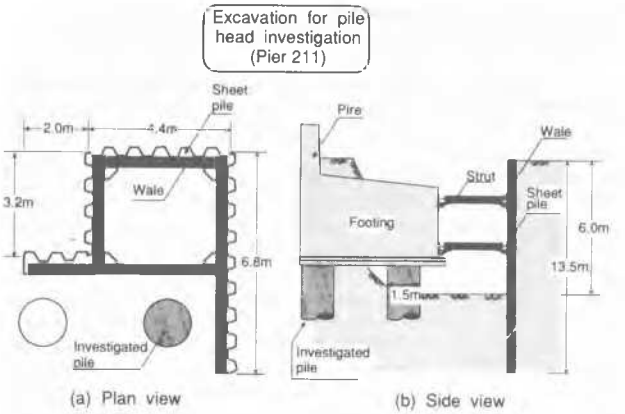

Fig.51 Details of the excavation work for investigating injury at pile head

Fig.52 Crack development at the pile head, Pier 211 (Hanshin Highway Authority, 1996)

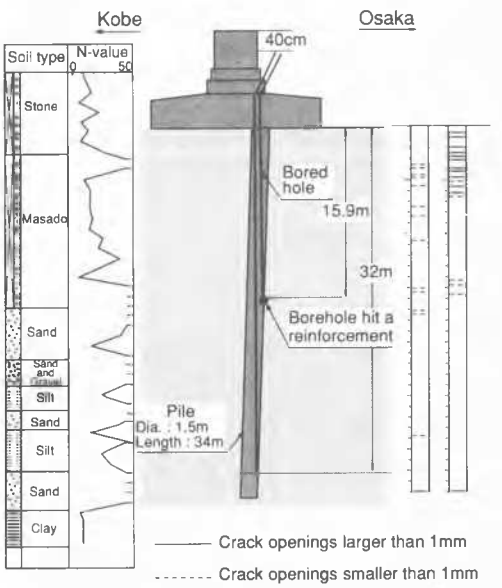

Fig.53 Scheme of core boring and inspection by a borehole camera

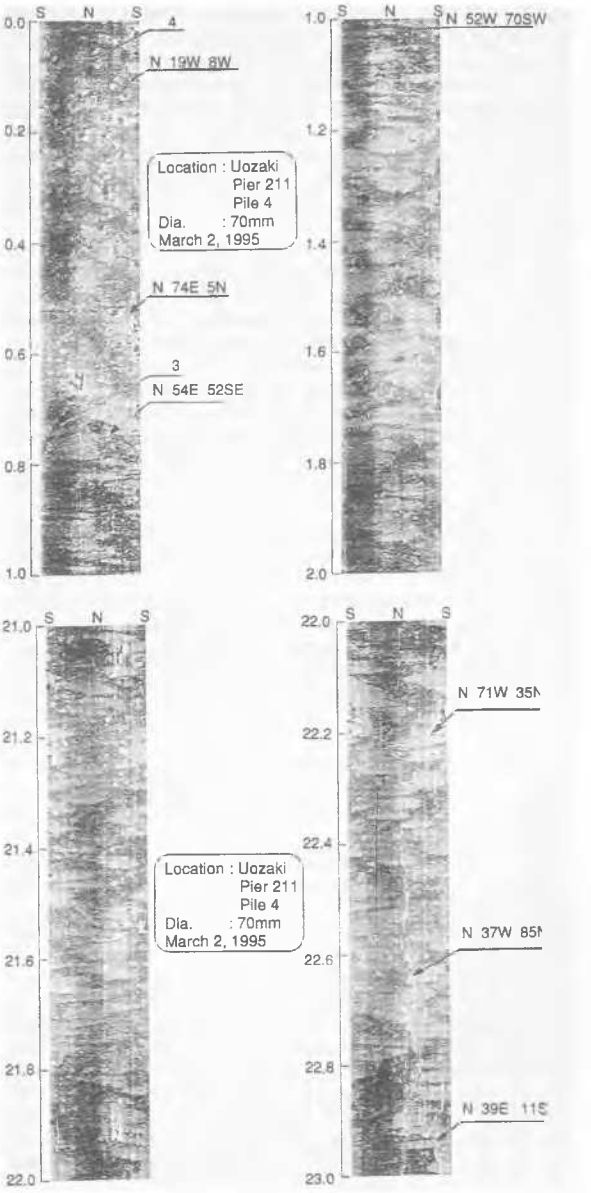

Fig.54 Feature of crack development at the pile head and mid-depth of the pile (Hanshin Highway Authority, 1996)

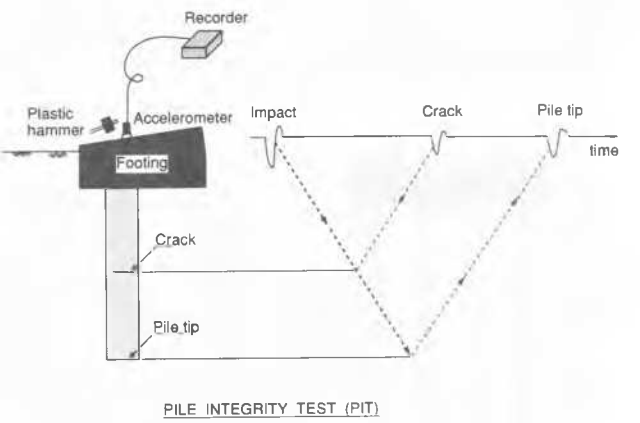

Fig.55 Illustration of pile integrity test (PIT)

provided. It is also noted in Fig.56 that the number of cracks is large at depths between 16m and 22m for the pile P3 and at depths 9 to 15m for the pile P5. The reclaimed Masado soil at this site is considered to have developed liquefaction to a depth of about 20m, leading to considerable softening of this layer as against the non-liquefied soil deposits below the depth of about 20m. Thus, it is highly likely that the magnitude of bending moment became large near the interface of these two layers.

The outcome of the in-situ investigations as above revealed the fact that, generally speaking, the pile damage had taken place around the three depths illustrated in Fig.57. In practically all the piles investigated, cracks were detected at depths 0 - 3m below the bottom of the footing slab. The damage at the pile head was supposedly caused by a great magnitude of bending moment resulting from the inertia force from the superstructure during intense shaking at the time of the earthquake. The cracks near the interface between liquefied and unliquefied deposits were observed mainly in the piers located near the waterfront. The cracks were also observed at the depths where design was made to reduce the cross sectional area or reinforcement. This type of damage was identified, by and large, in the case of the piles located in proximity to the waterfront. Thus, it may be considered that the cracks at some depths were caused by the lateral spreading of the surrounding soils that had liquefied during the main shaking of the earthquake.

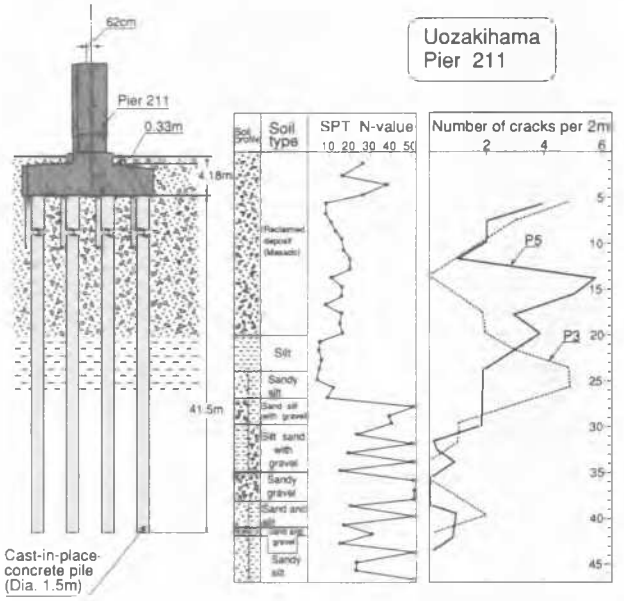

Fig.56 Observed number of cracks per 2m length of the piles (Hanshin Highway Authority, 1996)

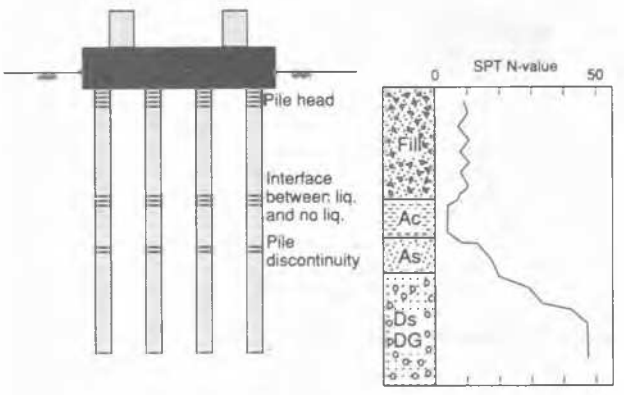

Fig.57 Three locations in the pile body where cracks were predominantly observed

DAMAGE TO FOUNDATIONS IN THE STORAGE TANK FARM

There are several tank farms for storage of oil and liquefied propane gas (LPG) in the man-made islands in the port area of Kobe. Storage tanks with various capacities were shaken very severely and affected more or less by the ground damage due to liquefaction. However, it was fortunate that despite the enormous damage to structures and foundations, the loss was only monetary and none of feared scenarios such as breakout of fire has occurred. Among several farms, the storage tanks and facilities in Mikagehama Island are those investigated in details as to the effects emerging from the liquefaction of the ground. The outcome of extensive studies made in this island will be presented in details. The location of the tank farm is shown in Fig.19. Detailed layout of tanks and other related facilities is shown in the map of Fig.58. As indicated, the triangular section in the southeast part is occupied by tanks and other related facilities for storage of LPG. The rest of the area in the northwest part is used for oil storage tanks. The LPG unshipping berth is located in front of the southern revetment and the berth for oil loading and unloading is located at the western revetment.

As a result of extensive liquefaction, lateral spreading took place over the island causing sand boiling, cracking in the premise of the LPG yard and settlements of the ground. The overall features of the ground cracking are demonstrated in terms of a sketch in Fig.59. It may be seen that there are depressions just behind the quaywalls accompanied by the large ground movements. Fissures or cracks are seen in the figure having developed farther inland from the waterfront.

1 Soil Conditions

Site investigations including SPT and tube sampling were conducted before and after the earthquake at various locations in the premise. Fig.58 shows the places where boring were performed to identify soil profiles. One of the soil profiles at a place in the center of the LPG Tank101 is shown in Fig.60 where it may be seen that the man-made Masado deposit consisting of sand with silt and gravel exists down to a depth of about 15m. The soil materials were taken from the weathered granite deposits at the foothill of the Rokko Mountain behind the Kobe city area. Underneath the reclaimed deposit, a layer of silty clay exists which is the seabed deposit before the reclamation was made in 1960's. It appears likely that the gravel containing silty sand had developed liquefaction due to the intense shaking during the earthquake.

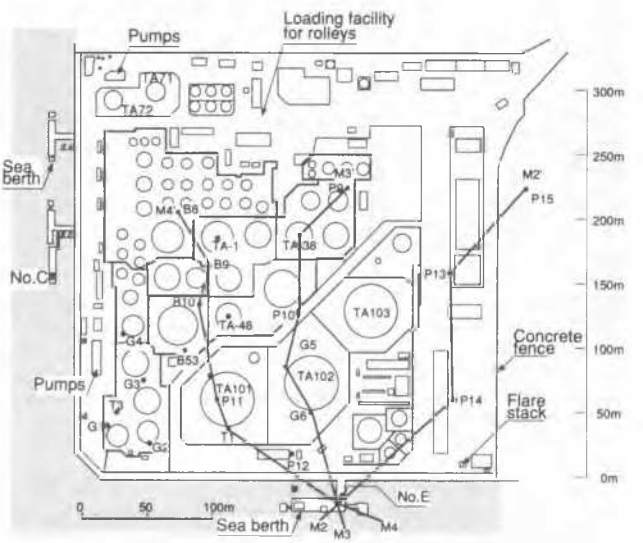

Fig.58 Map of the LPG tank location

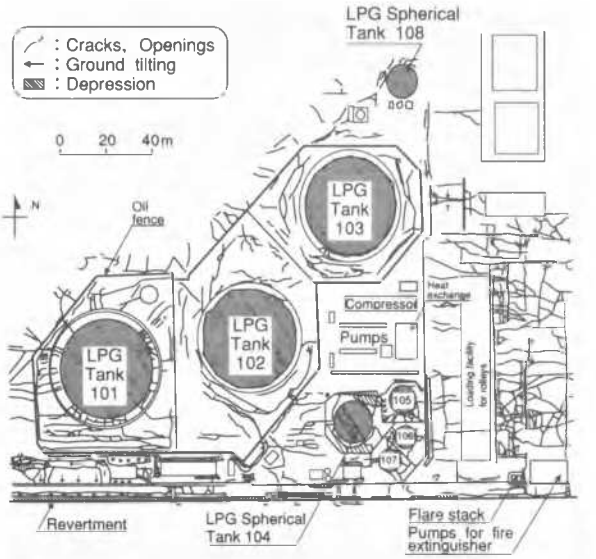

Fig.59 Ground distorsion in the tank farm (High Pressure Gas Institute, 1995)

In order to visualize overall features of soil profile, pictures of soil stratification through some cross sections were drawn based on individual soil profile data at several points. A cross sectional view through the sections M2-M2' and M3-M3' are shown in Fig.61 where it may be seen that, while the depth is variable to some extent, the reclaimed fill composed of Masado prevails to a depth of approximately 15-20m all over the island. The SPT N-values are low on the order of 10 to 15 and as such the reclaimed soils were under conditions susceptible to liquefaction. Underneath the reclaimed fills there exist a silty clay deposit in original seabed.

2 Lateral spreading of Mikagehama Island

Lateral spreading of the terrain was investigated by the method of the ground surveying as described previously. Four alignments chosen for surveying are shown in the inset of Fig.62. The alignment M-1 was along the concrete fence separating the premise from the other storage yard on the east. Alignment M-4 was chosen in the premice due south of the LPG Tank101. Shown in Fig.62 are the features of ground distorsion along the cross section M-3 where it may be seen that the lateral displacement at the ground surface occurred through a distance of 95m inland from the waterfront.

3 Damage feature of flat-bottom cylindrical LPG tanks

One of the LPG tanks (No.101 in Fig.59) with a storage capacity of 20,000 kℓ sustained damage at the outlet-inlet nozzle (exit of liquefied gas) installed at the flank, leading to leakage of liquefied natural gas. At the time of the earthquake, this tank contained about 6,700 kℓ of LPG and about half of the gas leaked in the premise enclosed by protection fence. The remaining half was transferred to an other uninjured tank. Luckily enough, inflammable content did not catch fire, and, therefore, a disastrous scenario was avoided. Some of the evaporated gas is purported to have dispersed in the air due to wind blowing towards south and the rest of the gas seems to have seeped into the ground through fissures of the ground created by the liquefaction.

The cause of the leakage was explained as follows. (High Pressure Gas Institute, 1995). A tall steel trestle had been installed outside the tank to hang up the emergency shut-off valve which was connected to the outlet nozzle pipe, as illustrated in Fig.63. This new installation was carried out some years after the start of the tank operation to ensure further safety. The steel trestle was resting on a simple concrete block embedded in the ground to a depth of about 1.5m. Owing to the liquefaction, the ground moved seawards about 70cm. The concrete block also settled about 70cm accompanied by sinking of the trestle. As a result, all the weight of the trestle was then applied as an external load to the emergency shut-off valve. This vertical load was transmitted to the inlet-outlet pipe rigidly connected with bolts to the frank of the LPG tank. Because of the excessive weight vertically applied, bolt-fastened flange of the rigid inlet-outlet pipe was forced to open slightly and this led to the leakage of LPG following the earthquake. It is apparent that this incident was caused by the large settlement of the concrete block supporting the trestle. As the pile-supported tank body remained unsettled, the relative settlement as much as 70cm occurred between the tank and trestle. This incident left an important lesson that the foundation of auxiliary facilities should have been supported by a common foundation with the tank body.

In spite of the leakage, no serious damage was incurred to the structure of the Tank101. One of the measures of the structural damage would be the magnitude of tilt or differential settlement of the tank body. Shown in Fig.64 are the results of measurements of settlements. At 14 points around the tank equally spaced along its periphery, elevations were measured. The elevations are plotted in this figure versus expanded locations of measurement points along the periphery. The tilt of the tank is normally defined as the maximum difference of settlements at any two points divided by the diameter of the tank. For the post-earthquake conditions, the tilt is obtained as 8cm/3,889cm=0.21% as accordingly indicated in Fig.64. With reference to the pre-earthquake tilt similarly calculated, it means that there has been practicably no change in the tilt following the quake. According to the regulation by the Japanese Government, the allowable maximum tilt for the normal condition of operation is stipulated as being 1%, may it be prior to or after the quake. Consequently, the measured tilt for this tank was within the limit of the allowable tilt.

The foundation of the Tank101 consists of 97 cast-in-placed reinforced concrete piles installed by using Benoto excavation machine. The arrangements of the piles in plan and side views are shown in Fig.65. Each pile has a diameter of 1.1m and is embedded to a depth of 27m where a stiff deposit of gravel is encountered as shown in the soil profile of Fig. 65. Note that the soil profile shown was obtained at the center of the tank before the construction.

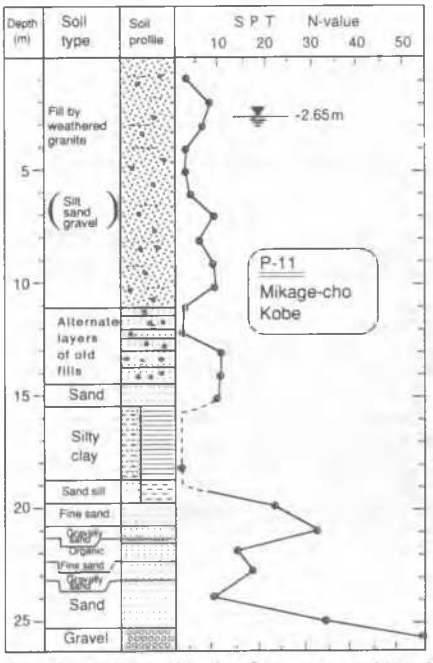

Fig.60 Soil profile in the center of Tank101

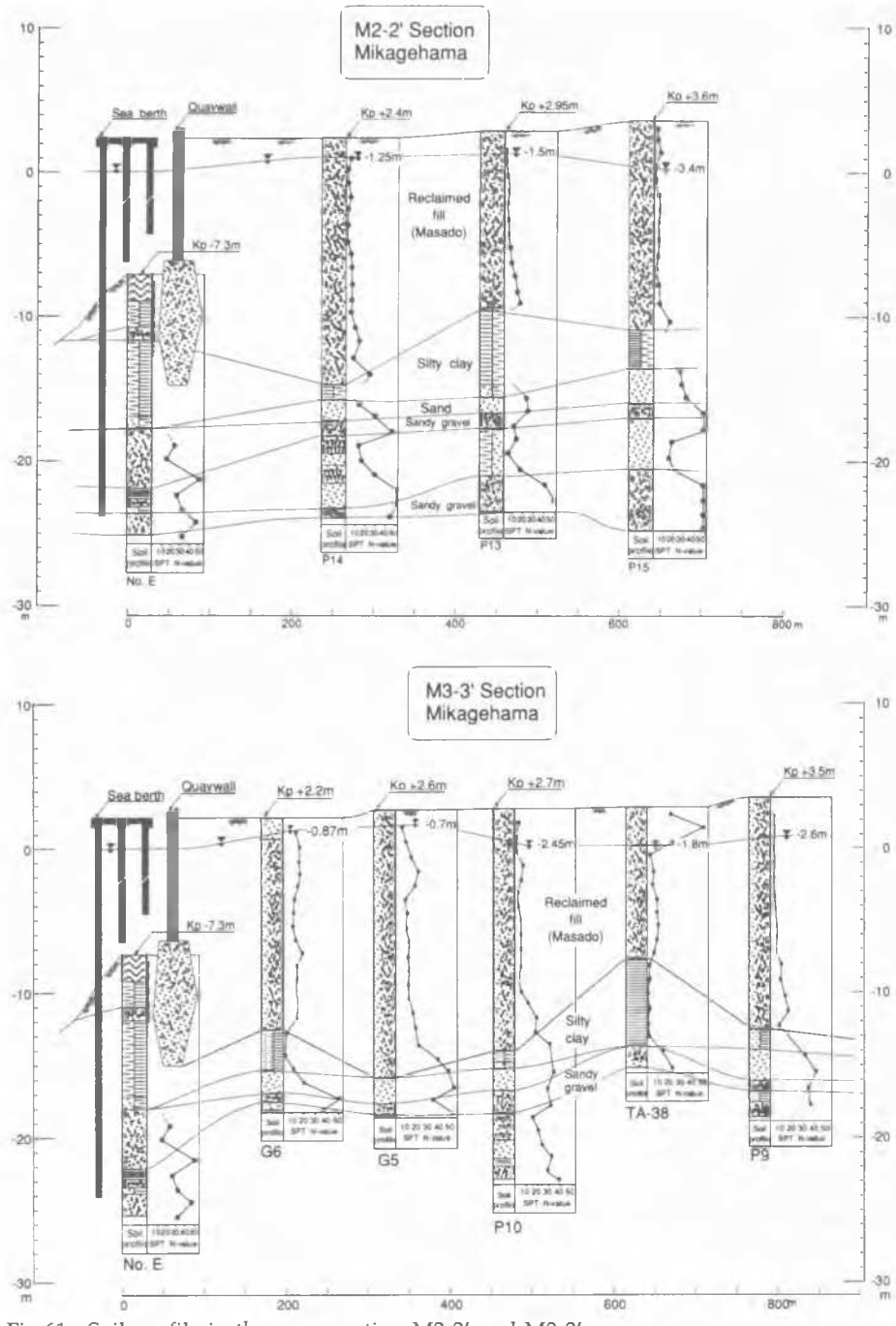

Fig.61 Soil profile in the cross section M2-2′ and M3-3′

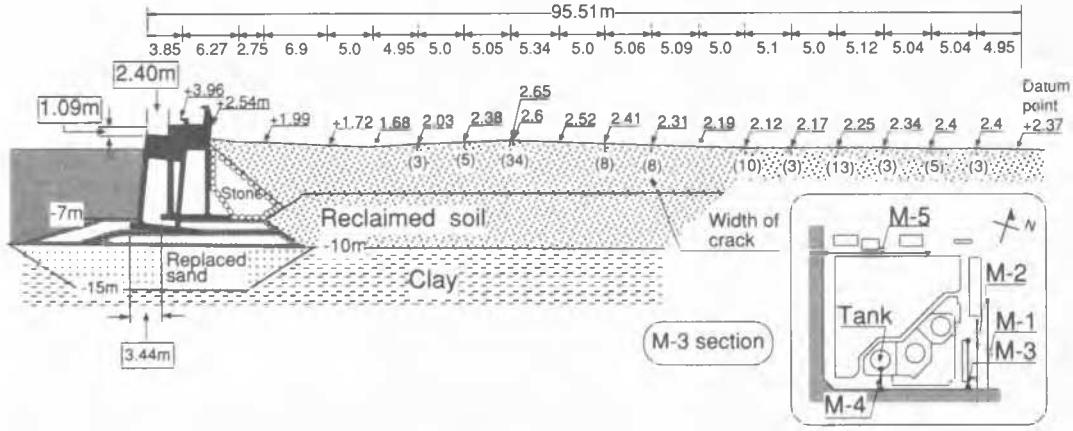

Fig.62 Ground distorsion in section M-3 at Mikagehama Island as measured by the ground surveying

To inspect soundness of the foundations, excavation was made after the earthquake underneath the Tank101 all over the plan area to a depth of 2m where the ground water table was encountered. No damage was whatsoever was discovered in the underground horizontal beams. Only small injury was horizontal cracks a few millimeters wide which had developed on the surface of several piles about 50cm below the tank slab. The surface concrete was scraped off to expose reinforcements inside, but no injury were identified further deep. To ensure sound functioning of the foundation, retrofit work was implemented to each pile. Reinforcement was conducted by enclosing each pile head by steel plates to a depth of 2m from the pile top.

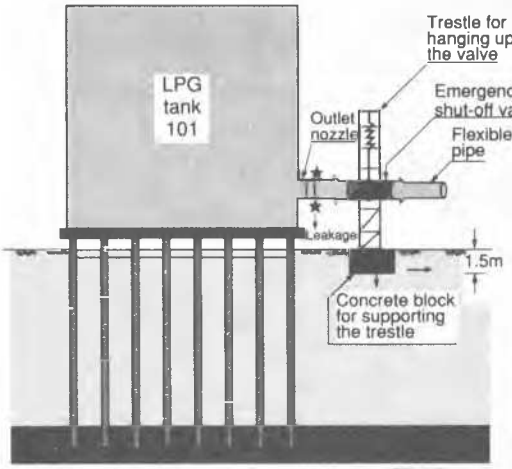

Fig. 63 Illustration for the gas leakage due to the differential settlement between the trestle and the LPG tank

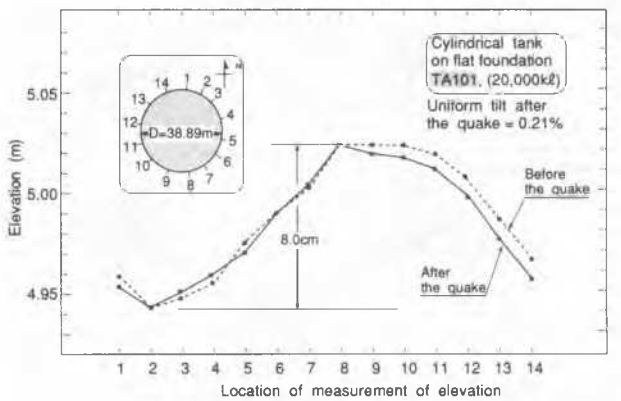

Fig. 64 Measurements of elevation along the periphery of the Tank101

Other cylindrical tanks No.102 and 103 having a 20,000 kℓ storage capacity were constructed on flat foundation lying directly on the ground compacted by means of the vibrofloatation. Plan and side views of the tanks are shown in Figs.66 and 67 where it is seen that a reinforced concrete circular ring is placed on the ground enclosing compacted soil fills inside. On top of the reinforced concrete slab inside the ring, a circular steel plate was placed as a bottom plate of the tank. The scheme of soil compaction by the method of vibrofloatation is displayed in Fig.66. A total of 1261 piles with a spacing of 1.4m were installed to a depth of 7.0m. It is to be noted that the plan area of compaction protruded horizontally by 6.0m out of the tank rim. In the Tank102 and 103, the outlet nozzle was connected, in a way similar to the Tank101, to an emergency shut-off valve which was supported by springs hanging from the top of a trestle. The trestle was placed on a concrete block foundation which sits on the compacted zone outside the tank. Unlike the Tank101, little differential settlement occurred between the tank and the

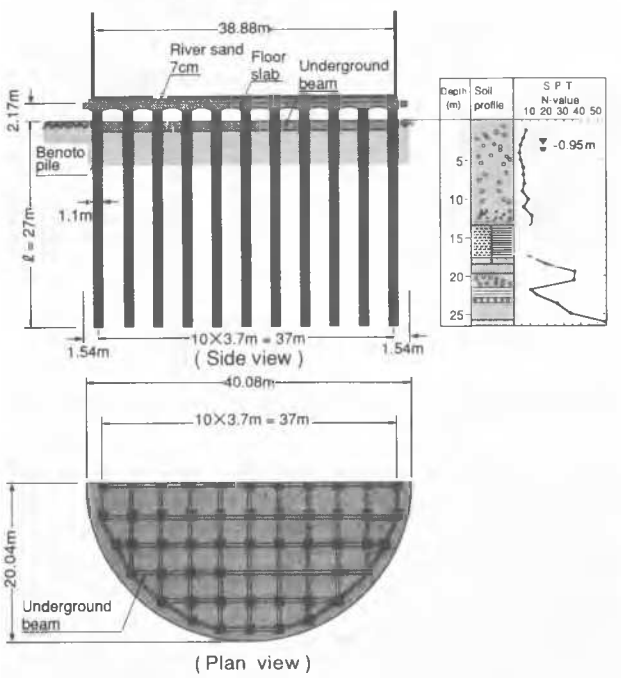

Fig. 65 Side and plan views of the foundation pile layout for the cylindrical Tank101

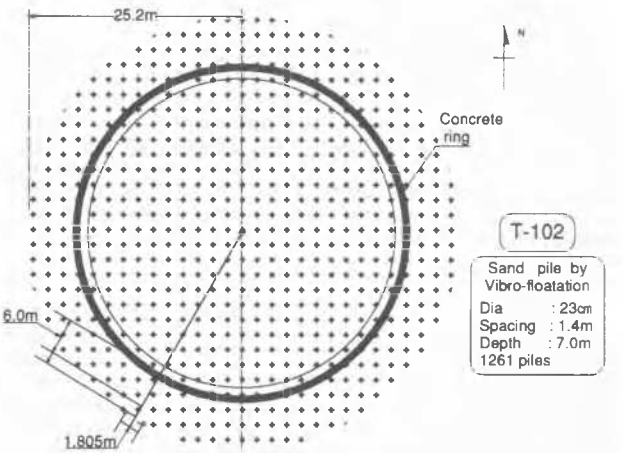

Fig. 66 Plan views of the ground improvement scheme for the cylindrical Tank102

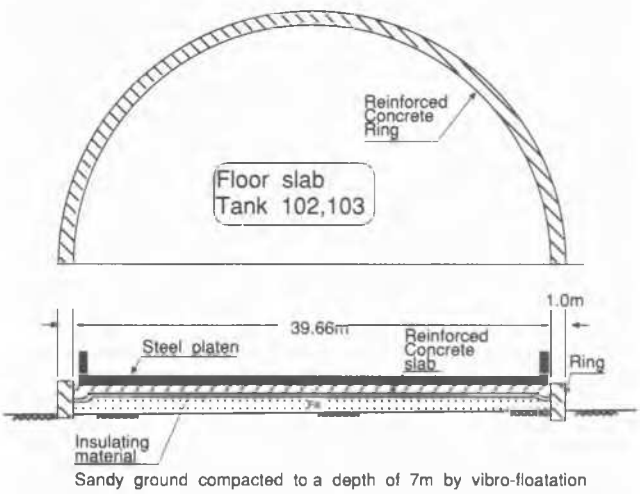

Fig.67 Side view of the foundation for the cylindrical Tank102

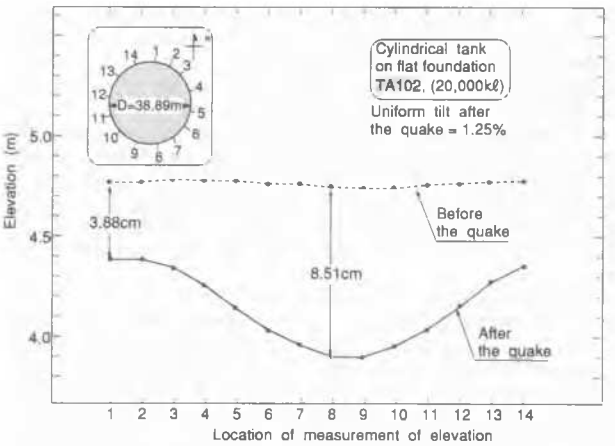

Fig.68 Measurements of elevation along the periphery of the Tank102

foundation of the trestle, because of both sitting commonly on the compacted ground. Needless to say, there was no gas leakage in the Tank102 and 103.

The elevation along the periphery of the tanks was measured prior to and after the earthquake as displayed in Fig.68 where the elevation at each point for the Tank 102 is plotted versus the location of measurements. Fig.68 shows that the maximum difference in elevation after the earthquake was 4.8cm for the Tank102, giving a value of tilt as being 1.25%. This value was in excess of 1.0% which is stipulated as an allowable limit in the government regulation. The tilt of the Tank103 was 0.34, a value within the allowable limit.

With the tilt beyond the acceptable limit, retrofit work was implemented for the Tank102 to level off the differential settlement. A total of 98 jacks each with a lift capacity of 20tons were placed along the periphery at the tank bottom and the tank body weighing about 2000tons was lifted up 1.5m. After compaction by small compactors and flattening of the ground surface, the huge tank body was lowered back to the original position. No retrofit work was done for the Tank103.

4 Damage feature of spherical LPG tanks

Four spherical tanks with a capacity of 100 to 1200 kℓ located in the southeast part of the premise suffered damage involving mainly tilts due to lateral spreading of the ground. Plan view of four spherical tanks are shown in Fig.69. Plan view of the foundation for the tank TA106 with a storage capacity of 100ton is shown in Fig.70 where it can be seen that the footing of each column is supported by four reinforced concrete piles (RC-pile) 30cm in diameter. The details of the footing with connecting underground beams are shown in Fig.71. The piles were driven to a stiff soil stratum at a depth of 20m. The soil profile near these tanks is shown in Fig.72 which is the boring data at a site P14 in Fig.58. The elevation along the periphery of each spherical tank was measured in the same fashion as in the case of the cylindrical tanks. The results of measurements for the Tank106 and 107 are displayed in Figs.73 and 74, where it can be seen that the differential settlement of the order of 27cm did developed in the pile of Tank106 resulting in the tilt as much as 3.6% which is apparently beyond the acceptable limit. The tank TA107 also suffered a tilt of 1.25% which was beyond the allowable limit. The tank TA106 and 107 were retrofit by excavating the ground to a depth of existing footing and by installing additional piles outside the existing footing.

Features of the damage to the pile foundation of TA106 and 107 were investigated in conjunction of the retrofit work where excavation was carried out to a depth of about 2.0m to remove the footing slabs. Locations of the two piles investigated are shown in Fig.69. Pile heads were exposed and the hole in the pile cross section was washed to remove soil debris inside. A

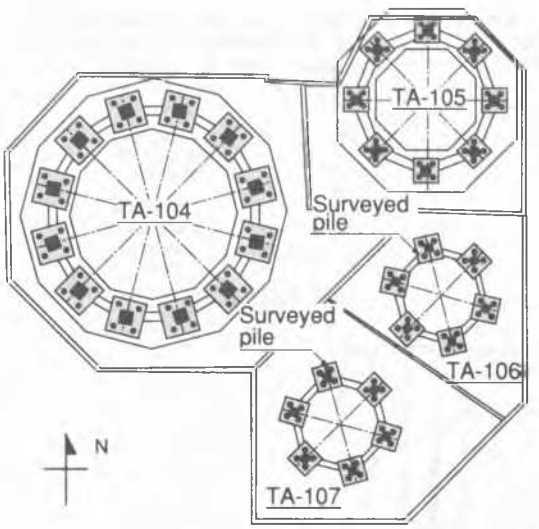

Fig. 69 Plan view of the foundations for the spherical tanks 104, 105, 106 and 107

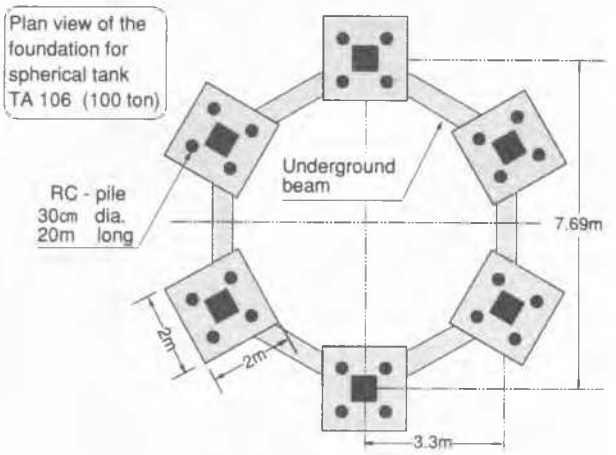

Fig. 70 Plan view of the foundation for cubic Tank106 and 107

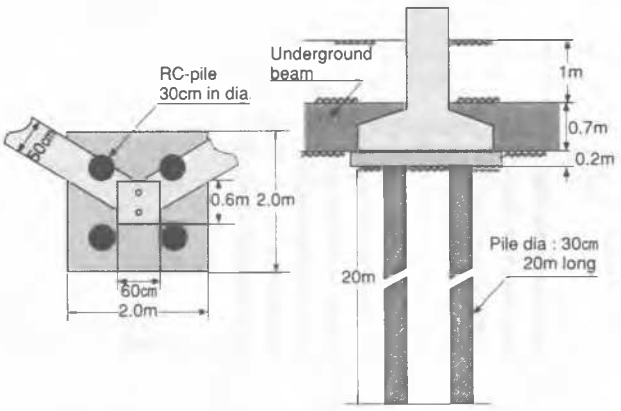

Fig. 71 Details of the foundation of spherical tanks

video camera was lowered into this hole to examine development of cracks around the wall. Results of the survey are presented in Figs. 75 and 76 where it may be seen that cracks developed predominantly at depth between 5 and 10m. Unfortunately, it was not possible to pull down the camera lower than 10m because of clogging of the hole. In addition, survey of pile deformation was carried out by lowing an inclinometer successively down the hole. By integrating the measured data on tilts through the depth, configuration of deformed piles was obtained as shown in Figs. 75 and

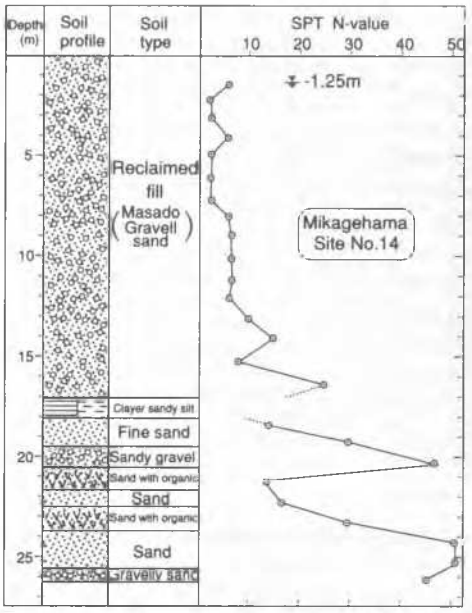

Fig. 72 Soil profile at a site near the spherical tanks106 and 107

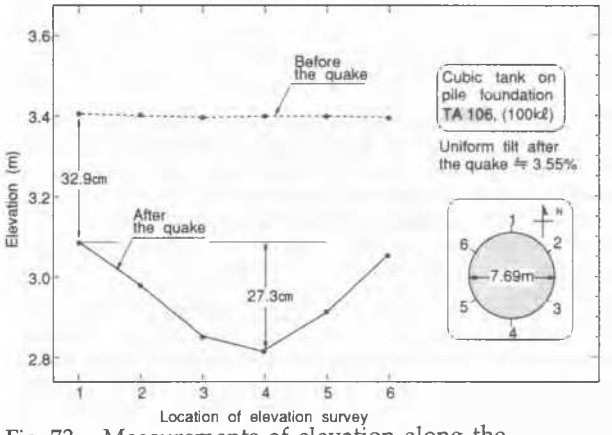

Fig. 73 Measurements of elevation along the periphery of the Tank106

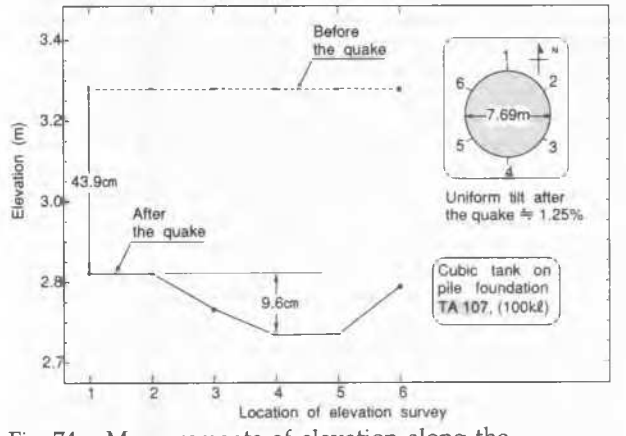

Fig. 74 Measurements of elevation along the periphery of the Tank107

76, where the relative magnitude of lateral deformation is displayed with respect to the deformation at the pile head chosen as being zero. These figures disclose the fact that the pile head moved predominantly towards the south about 50cm relative to the depth of 10m. The direction of this relative displacement can be seen more directly in the plan views of Figs. 75 and 76 where trajectories in plan are drawn. Unfortunately there is no documented record left as per visual observation of injury at the pile-head and around its connection to the footing.

SIMPLE ANALYSIS OF PILE-SOIL INTERACTION

1. General Concept

When piles are subjected to a shaking during earthquakes, they move back and forth horizontally almost in union with the movement of the surrounding ground. During the main shaking, sandy soils in a deposit have not yet softened so significantly due to liquefaction that relative movement between the piles and the ground would be small. However, there are chances for the piles to be damaged, if the ground motion is sufficiently large and consequent development of bending moment within the piles is great enough to become equal to a limiting value. It is to be noticed that the damage to the piles under the above loading conditions takes place in the upper portion of the pile near the head because of the bending moment becoming maximum around this portion. Since the load comes from the inertia force of superstructures, the influence of seismic loading may be referred to as "top-down effect".

It has been known that onset of liquefaction takes place approximately at the same time as the instant when peak acceleration occurs in the course of seismic load application having an irregular time history. Following the onset of liquefaction the once softened sandy material starts to move horizontally, if the ground is inclined. Under such conditions, lateral force would be applied to the pile body embedded in the ground, leading to downslope deformation of the pile. At this time, the seismic motion has already passed its peak, but the shaking may still be persistent in lesser intensity or has completely subsided. Therefore, the lateral force transmitted from superstructures due to inertia of seismic motion would be of insignificant magnitude and major load would be the lateral force coming directly from the soils surrounding the pile. Under such loading conditions, the maximum bending moment induced in the pile may occur not near the pile head but at a lower portion at some depth. Thus, the effects of earthquake loading are manifested in the form of lateral deformation of the ground imposing a significant force to the embedded portion of the pile, and as such the influence of seismic loading may be referred to as "bottom-up effect".

In summary, the effects of seismically induced loading to foundations such as piles are two fold. One is associated with the dynamic loads at the time of main shaking coming from the inertia force of superstructures which are applied to the top of the pile. As a result of such a top-down load transfer, the maximum bending moment and consequent damage tends to occur near the pile head. The other is related with the static loads emerging from the liquefaction-induced lateral movement of surrounding soil deposit. These loads are applied to the middle portion of the pile during the period of time after the main shaking of earthquakes is over. As a result of such a bottom-up mode of load application, the maximum bending moment and consequent damage tends to occur in the middle portion of the pile at a certain depth.

2. Analysis of piles subjected to lateral spreading of the ground

A simple analysis can be made for a pile by assuming it to be connected to a spring system, as shown in Fig.77, which is arranged to represent an interaction characteristics between piles and surrounding soil deposit. In this model, the spring constant, K, is obtained by multiplying the coefficient of subgrade reaction, k by an effective width of the pile, d,

$$K=kd \quad \text{.....(1)}$$

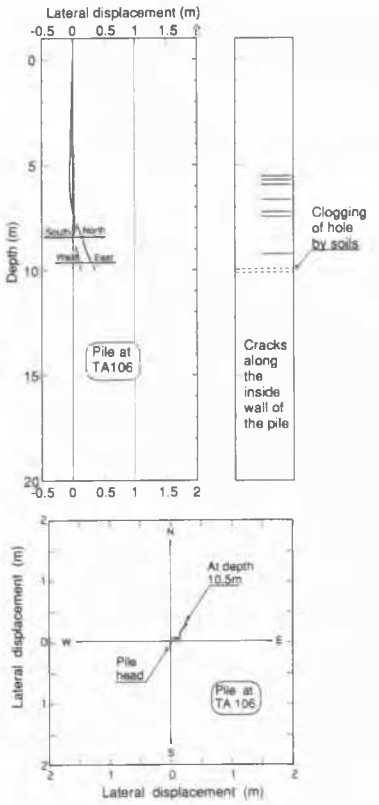

Fig.75 Lateral displacements of the pile at the Tank106 and features of crack development as identified by the video camera

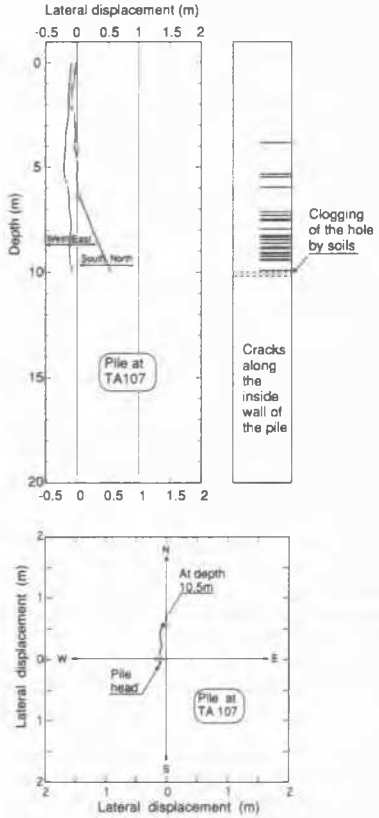

Fig.76 Lateral displacements of the pile at the Tank107 and features of crack development as identified by the video camera

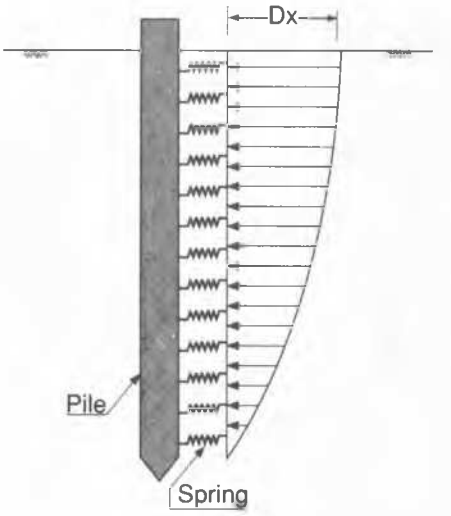

Fig.77 Model for the pile-soil interaction analyses

The coefficient, k, is defined as the ratio between the lateral force F per unit area and the difference between the lateral displacement of the pile, Up, and that of the free-field ground, U_G.

$$k = \frac{F}{Up - U_G} \quad \text{.....(2)}$$

It is to be noticed that the value of U_G should be chosen as the displacement of the ground sufficiently far away from the pile such that it is free from any interaction effects between the ground and the pile. To determine the coefficient of subgrade reaction to be utilized in the routine practice, several empirical formulae are suggested in the Japanese design code of bridge foundations. The most frequently used for sandy deposit is via the Young's modulus estimated from the SPT N-value. While there are numerous factors associated with uncertainty in determining the k-value, there is no other way at this moment but to rely upon the N-value. The k-values used herein and those estimated from the N-value.

The outcome of monitoring the pile deformation by virtue of a slope indicator for piles at the spherical tanks was described in the forgoing section. At this location, SPT k-values are assumed to be distributed though the depth as shown in Fig.78 on the basis of the soil profile data in Fig.72 which was obtained at a nearby site P14. With reference to the SPT N-value, the spring constants in normal conditions without liquefaction were assumed to take values of 11.2, 16.8 and 28.0 MN/m^2, for the reclaimed deposits as accordingly indicated in the figure. The deformation characteristics of the prefabricated reinforced concrete pile are expressed, as shown in Fig.79, in terms of a relation between the bending moment and curvature. This relation was derived from the given characteristics of the cross section specified by the pile manufacturer. It may be seen in Fig.79 that the pile is regarded to reach a point of yielding at a critical moment of Mc=2.45tf m with a curvature of $\phi = 0.0019/m$ where hair cracks are supposed to develop. At the maximum bending moment of 4.17tf m, the pile is considered to develop failure with a curvature of $\phi = 0.0204/m$. The non-linear nature of pile behaviour as described in Fig.79 was taken into account in performing the back analysis. The method of analysis adopted herein consists of a series of calculation as follows.

(1) First, lateral displacement of the soil deposit is prescribed throughout the depth. In the case of the spherical tank site TA106 and 107, the reclaimed Masado

soil is postulated to have developed liquefaction to a depth of 17m, and the entire soil mass above it to have moved with a sinusoidal distribution of lateral deformation as illustrated in Fig.77.

(2) The lateral displacement on the ground surface was assumed to have been 2.4m. This is based on the data obtained by using the ground surveying method as described above. As shown in the inset of Fig.62, the alignment of the ground surveying at the cross section M-3 is the one closest to the site of the spherical tank site being considered. Distribution of the lateral displacement along the section M-3 is obtained as shown in Fig.80 based on the data displayed in Fig.62. Since the location of the spherical tanks is approximately 30m inland from the quaywall, the lateral displacement on the ground surface may be read off as being about 2.4m. The lateral displacement within the liquefied stratum is assumed to have a distribution represented by a sine function to the depth of 17m as shown in Fig.77.

(3) The displacement of the ground as postulated above was applied to the equivalently-linear spring in the soil-pile model as shown in Fig.78 and analysis was made for the spring-supported beam to obtain lateral displacement of the pile. In doing so, the lower end of the pile was assumed to be fixed, and the pile head was postulated to be fixed to the footing but free to move in the horizontal direction. In the analysis, the spring constants at each depth were reduced in a wide range from 1 to 5×10^{-4}. The factor by which the coefficient of subgrade reaction or spring constant is reduced will be called "stiffness degradation factor" and denoted by β.

(4) As known from Fig.72, the ground water table at this location was 1.25m below the surface. The partially saturated soil above it, plus a thin layer of 0.85m below it, may be assumed not to have developed liquefaction. Thus, the 2.0m thick surface layer is envisaged to have moved together with the underlying layer which has undergone the lateral spreading. It may be assumed, therefore, that a passive earth pressure of $K_p\gamma_t H^2/2$ is applied to the soil block 2.0m in thickness near the surface, where $K_p = \tan^2(\phi/2+\pi/4)$, H=2.0m, ϕ=37° and $\gamma_t = 1.85 tf/m^3$, were assumed for calculation.

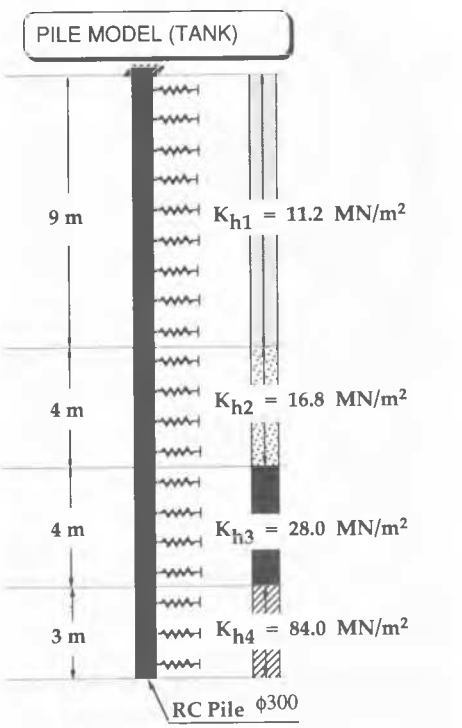

Fig.78 A model of soil-pile interaction

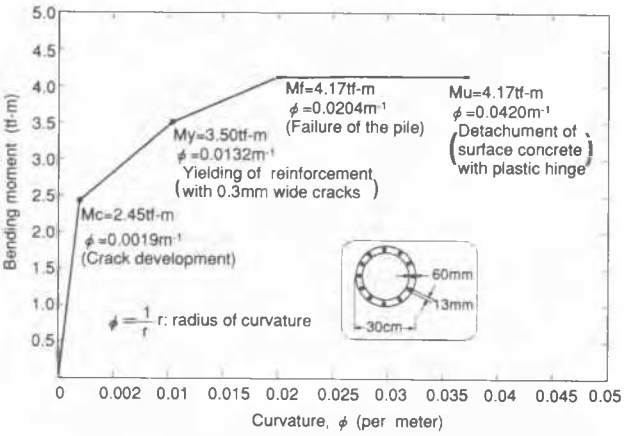

Fig.79 Elasto -plastic relation between the bending moment and curvature of the pile used for the foundations of Tank106 and 107

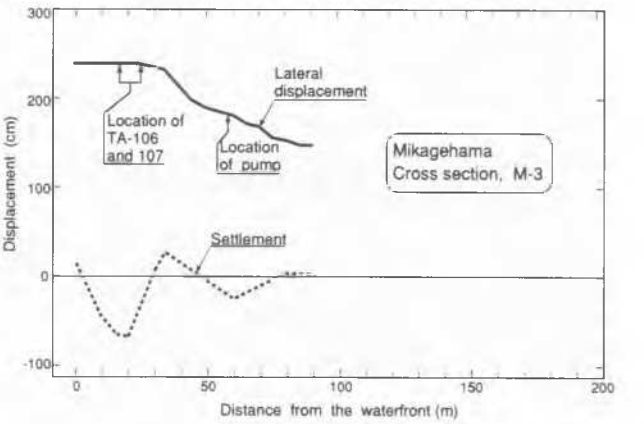

Fig.80 Ground displacements in LPG tank farm

(5) The foundation of the Tank106 and 107 consists of 6 raft footings each supported by 4 piles as indicated in Fig.69. As such, a total of 24 piles is considered to have experienced lateral spreading. However, 8 piles connected to 2 footings in the southern side may be assumed not to have been influenced significantly by the lateral force due to flow deformation of liquefied soil. Thus, the remaining 16 piles are assumed to have been subjected to the lateral force. Now, assuming the gross width of the foundation frame to be 8m as indicated in Fig.70, the total earth pressure acting on the foundation system would be estimated as $8m\times K_p\gamma_t H^2/2$. Then, the force applied to each of the 16 piles is obtained as $8/16\times K_p\gamma_t H^2/2 = K_p\gamma_t H^2/4$. In the analysis, the passive earth pressure of this magnitude was applied to the pile head near the surface, along with the displacement distribution as mentioned above.

The outcome of the analysis is demonstrated in Fig.81 for variously assumed values of β. In view of the severe devastation near the ground surface observed at the time of the earthquake, it was considered appropriate to reduce the stiffness of the liquefied layer significantly. Thus, the value of β was changed in three steps from 2×10^{-3} to 5×10^{-4} as accordingly indicated in Fig.81.

It is apparent, though not shown so in Fig.81, that, when the spring contents take the values stipulated in

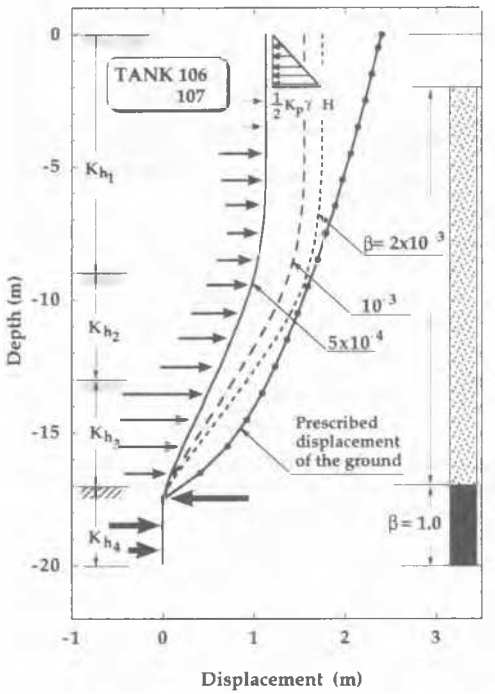

Fig.81 Comparison of computed pile displacement with the assumed soil displacement for the piles of Tank106 and 107

the design code, the pile moves in unison with the movement of the surrounding soils and there is no relative displacement between the pile and the soil deposit. If a degradation of $\beta = 2\times10^{-3}$ is introduced, the analysis result shows a pile movement of 1.75m on the surface as indicated in Fig.81. If the degradation of 5×10^{-4} is introduced for the stiffness in the liquefied stratum to a depth of 17m, the movement of 1.1m is obtained for the pile on the ground surface. The direction of the force acting on the pile body is indicated in Fig.81 with arrows where it can be seen that the moving soils in the liquefied layers is generating driving force in the direction of pile movement, whereas the underlying unliquefied soil deposit with $\beta = 1.0$ is resisting by mobilizing the force acting in the opposite direction.

The deformation of the piles as measured by the inclinometer does not yield absolute values of actual deformations because of lack of measured data below the depth of 10m as indicated in Figs.75 and 76. Thus, the measured pile deformation should be interpreted as the data indicating the pattern of relative deformation above the depth of 10m. With this fact in mind, it would be appropriate to quote the measured pattern of deformation from Figs.75 and 76 and superimpose them in the diagram of calculated deformation in such a way that both of them become as coincident as possible. The comparison in this vein is demonstrated in the diagram of Fig.82 where it may be seen that the coincidence of the measured and estimated values is roughly achieved for the case of the stiffness degradation factor as low as $\beta = 5\times10^{-4}$ where the ground deformation on the surface is calculated to be 1.1m.

When performing the analysis, the bending moment in the pile body was calculated in such a way that it satisfies the pile stiffness characteristics as shown in Fig.79. The moment distribution versus depth obtained from the analysis is demonstrated in Fig.83. It may be seen that the bending moment induced in the pile is approximately equal to the level of the moment at which yielding starts to occur. Looking back at the features of crack development displayed in Figs.75 and 76, it may as well be mentioned that the depth of crack development roughly coincides with the depth range at which the bending moment becomes equal to its yield and failure value.

From the above consideration, it is noted that there are three points, as follows, to which estimated behaviour of the piles should be checked to verify if a chosen value of stiffness degradation parameter, β, is appropriate or not.

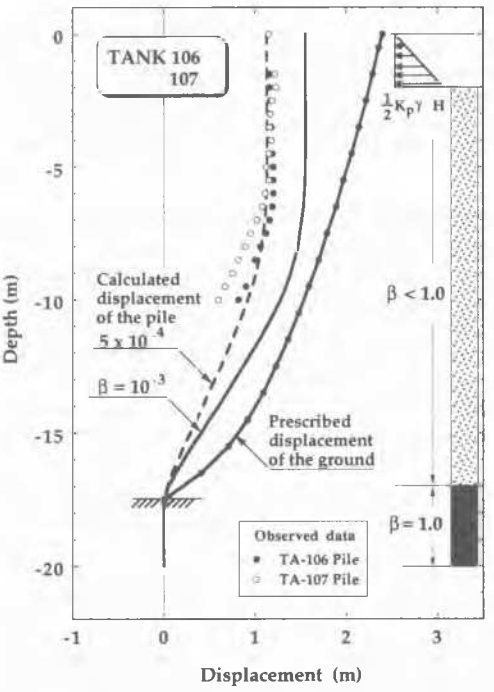

Fig.82 Comparison of calculated pile deformations with those measured by the inclinometer

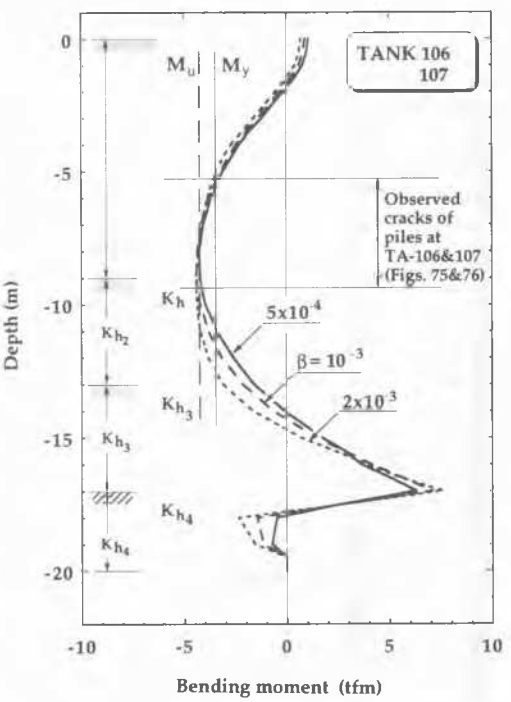

Fig.83 Calculated bending moment of the piles for the foundations of Tank106 and 107

(1) For the portion of the pile where cracks were observed by the video camera, the bending moment calculated from the analysis should coincide with the threshold moment of reinforced concrete at which yielding or subsequent failure can occur.

(2) The pattern of the lateral deformation calculated from the analysis should coincide with the deflection of the pile observed by the inclinometer.

(3) In a majority of the cases of pile damage due to lateral flow, the ground deformation has been observed to become greater than that of the pile head. In view of this, the deflection of the pile head calculated from the analysis should be significantly smaller than the ground surface deformation which is assumed as an input deformation at the beginning of the analysis.

For the case of the spherical tank foundation studied above, the first and second requirements seem to be satisfied roughly. In examining the third condition, it is necessary to know an absolute value of the pile head deflection resulting from the lateral flow, but unfortunately there is no available data to be referred to for the case of TA106 and 107 foundations. It would be of interest, however, to make proper reference to the compiled data regarding the movement of the ground and bridge piers obtained by the Hanshin Highway Authority. The lateral movements of the bridge piers along the No.5 Bay Route (see Fig.45) were monitored by virtue of GPS. The ground displacements in the vicinity were also measured by means of GPS or by using the airphoto interpretation technique. These two movements were plotted, as shown in Fig.84 for the data obtained from three types of foundations, that is, pile, caisson and diaphragm wall foundations (Iwasaki et al. 1996). It may be seen in Fig.84 that the lateral deformation of the pile-supported foundation was 50%, on the average, of the ground displacement in their neighbourhood, but this ratio could vary in the wide range between 15% and 80%.

For the particular case of the spherical tank foundations, the ratio of the pile head deflection to the nearby ground surface was computed in the above-mentioned analyses as being 1.75m/2.4m=73% for a stiffness degradation parameter of $\beta = 2\times10^{-3}$ and 1.1m/2.4m=46% for $\beta = 5\times10^{-4}$. In view of this, it may well be mentioned that the computed values of the pile deflection lie within a range of its possible variation which can be conjectured in the light of the other data obtained from observation of the bridge foundations.

The outcome of the case studies as above can provide a reasonable estimate of the range for the stiffness degradation parameter β that may be incorporated in the design practice. It is apparent that the parameter β is closely linked with the deflection of the pile head relative to the displacement of the surrounding ground. To examine this aspect, calculations were made for three values of β to obtain the deflection of the pile head, U_P, for an postulated value of U_G=2.4m in the case of the spherical tank foundations. The results of computation are plotted in Fig.85 in terms of the normalized relative displacement, $(U_G - U_P)/ U_G$ plotted versus the value of β. It may be seen that, if stiffness degradation parameter is larger than 3×10^{-2}, the relative displacement $U_G - U_P$ becomes practically equal to zero, indicating concomitant movement of the pile and the surrounding ground. If the β-value is reduced to a value as small as 5×10^{-3} to 5×10^{-4}, relative displacement becomes 20% to 60% of the ground displacement, respectively. Though not conclusive yet, it may be mentioned that the stiffness of

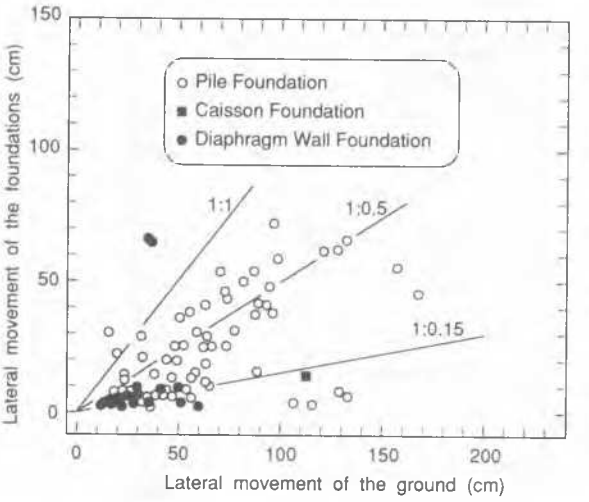

Fig.84 Relation between ground flow and foundation movement (Iwasaki, 1996)

the liquefied soils undergoing flow must have been reduced by a factor of $5\times10^{-3} - 5\times10^{-4}$ from the nominally assumed value without considering softening due to liquefaction. In view of the fact that the deformation characteristics of soils is replaced by an equivalent linear spring, the degradation parameter β is expected to change depending upon the magnitude of deformation assumed for the soil as an imput. This aspect may need to be deliberated further on.

For the design purpose, it might be of interest to see how much force has been applied laterally to the pile body from the surrounding ground for the case of the spherical tank foundations. The lateral force evaluated through the equation

$$F = k\beta(U_p - U_G) \qquad \text{.....(3)}$$

was normalized to the overburden pressure σ_v and plotted versus the depth in Fig.86. It may be seen that the lateral force applied to the pile body was of the order of 3 to 7% of the overburden pressure.

The consideration in the above is only one example of the case studies for the behaviour of piles subjected to lateral spreading of liquefied deposits. A number of cases of pile breakage may need to be studied along the line of reasonings similar to the above, before any conclusion is drawn regarding the lateral force to be allowed for in designing piles driven in deposits likely to develop lateral flow during earthquake.

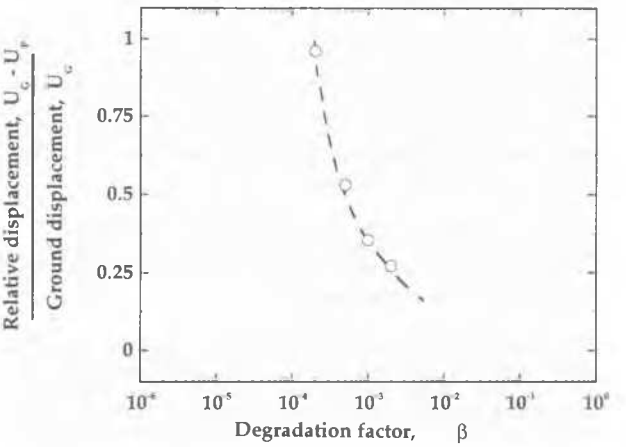

Fig.85 Relative displacement between piles and soil deposits as a function of stiffness degradation parameter β

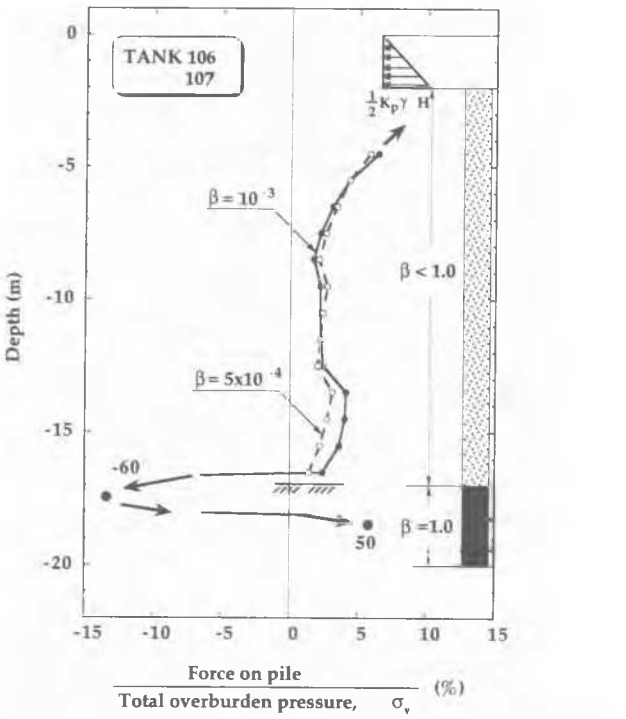

Fig.86 Computed lateral force acting on the piles from the soil deposit

CONCLUDING REMARKS

As a result of in-situ studies of soil conditions and damage features of LPG tanks at the time of the 1995 Kobe Earthquakes, concluding remarks may be addressed as follows.

1. Unlike many cases in past earthquakes, the soils composed of gravel-containing silty sands have developed extensive liquefaction in the reclaimed islands in Kobe. It was thus found that even soils with high uniformity coefficient containing about 50% of gravels could develop liquefaction if it is subjected to a high intensity of shaking

2. Beneficial effects of compaction by means of sand compaction pile and vibro-floatation techniques were found to be valid for such well-graded soils for preventing hazard due to liquefaction. This was substantiated by a higher value of cyclic strength of undisturbed samples from the compacted deposits as compared to that of undisturbed samples from uncompacted deposits.

3. The once liquefied soils were found to develop lateral spreading if lateral constraint is released in the soil deposits such as those behind the quaywalls which are displaced largely by seismic actions. The lateral displacement of the quaywall of the order of 2-3m was also shown to propagate rearwards in the backland through a distance of 150-200m.

4. The foundation piles for industrial facilities installed in the deposits undergoing the lateral spreading were shown to be subjected to lateral force, resulting in fatal injury in the pile body.

5. Simple back analyses were performed to evaluate the magnitude of the lateral force that had been applied to the pile body during the flow of the liquefied deposit. It was revealed that the value of the spring constant entering in the model of soil-pile interaction analyses must be reduced by a factor of 5×10^{-3} to 5×10^{-4} in order to provide a plausible explanation for the observed fact that the displacement of piles is about 15 to 80% of the far-field displacement occurring in the surrounding soil deposits.

ACKNOWLEDGMENTS

In preparing the manuscript for this lecture, the outcome of in-situ investigations conducted on foundations of bridge piers was provided by Mr. H. Ishizaki and Mr. Y. Egawa of the Hanshin Expressway Authority. The detailed soil investigations at the packing house in Port Island were performed by the Cooperative Research Committee organized by Dr. Y. Goto of Ohbayashi Co. The data on geology and geomorphology of the Kobe area were offered by the courtesy of Professor N. Adachi of Kyoto University. Dr. Y. Iwasaki and Mr. Y. Suwa of Osaka Geo-Institute kindly provided the seismicity data base recorded at the time of the Kobe Earthquake. The analyses of piles subjected to lateral flow of soils were performed by Dr. M. Cubrinovski of Kisojiban Consultants. The drafting of the manuscript was materialized by overall assistance of Dr. K. Mori and Mr. Y. Morita of Kisojiban Consultants. The author wishes to express his sincere thanks and deep appreciation to the individuals mentioned above.

REFERENCES

Fukushima, Y. (1995), "Empirical Methods of Input Earthquake Motions Based on Source and Transmission Mechanism of Earthquake Waves", Report of Ohsaki Research Institute.

Fujita, K. (1976), "The Quaternary tectonic stress states of Southwest Japan", Journal of Geosciences, Osaka City University, Vol. 20, pp. 93-103. (in Japanese)

Geotechnical Research Collaboration Committee on the Hanshin-Awaji Earth-quake (1996), Annual Report. (in Japanese)

Hamada, M., Isoyama, R., and Wakamatsu. K. (1996), "Liquefaction-Induced Ground Displacement and its Related Damage to Lifeline Facilities", Soils and Foundations, Special Issue on Geotechnical Aspects of the January 17, 1995 Hyogo-ken Nambu Earthquake, pp.81-97.

Hanshin Highway Authority (1996), "Investigation on the Seismic Damages of Bridge Foundations in the Reclaimed Land". (in Japanese)

Hatanaka, M., Uchida, A. and Ohara, J. (1997), "Liquefaction Characteristics of a Gravelly Fill Liquefied during the 1995 Hyogo-ken Nambu Earthquake", Soils and Foundations, Vol. 37, No.3, pp. 107-115.

High Pressure Gas Safety Institute of Japan (1995), "Interim Report of Investigation Committee on the LP-Gas Leakage from a Storage Tank Caused by the Kobe Earthquake".

Ishihara, K., Yoshida, K., and Kato, M., (1997), "Characteristics of Lateral Spreading in Liquefied Deposits during the 1995 Hanshin-Awaji Earthquake", Journal of Earthquake Engineering, Vol. 1, No. 1, pp.23-55, Imperial College Press.

Inagaki, H., Iai, S., Sugano, T., Yamazaki, H., and Inatori, T., (1996), "Performance of Caisson Type Quaywalls at Kobe Port" Soils and Foundations, Special Issue on Geotechnical Aspects of the January 17, 1995 Hyogo-ken Nambu Earthquake, pp.119-136.

Iwasaki,T. (1996), "Perspectives of Seismic Design Criteria for Highway Bridges in Japan", Special Theme Session on Seismic Design of Bridges, 11th

Word Conference on Earthquake Engineering, Acapulco, Mexico.

Japanese Geotechnical Society (1996), Report of Hanshin-Awaji Earthquake. (in Japanese)

Joyner and Boor (1988), "Measurement, Characterization and Prediction of Strong Ground Motion", Earthquake Engineering and Soil Dynamics II, GT Special Volume No.20, ASCE, pp.43-102.

Matsui,T. and Oda,K. (1996), "Foundation Damage of Structures", Soils and Foundations, Special Issue on Geotechnical Aspects of the January 17, 1995 Hyogo-ken Nambu Earthquake, pp.189-200.

Ministry of Construction (1995), Investigation Report on Highway Bridge Damage Caused by the Hyogo-ken Nambu Earthquake. (in Japanese)

Oh-oka, H., Onishi, K., Nanba, S., Mori, T., Ishikawa, K.,Koyama, S. and Shimizu, S. (1997), "Liquefaction-Induced Failure of Piles in 1995 Kobe Earthquake", Proc. of the 3rd Kansai International Forum on Comparative Geo technical Engineering (KIG-Forum '97), pp.265-274

Toki (1995), Committee of Earthquake Observation and Research in the Kansai Area. (in Japanese)

Tokimatsu, K., Oh-oka, H., Samoto, Y., Nakazawa, A., and Asaka, Y., (1997), "Failure and Deformation Modes of Piles Caused by Liquefaction-Induced Lateral Spreading in 1995 Hyogo-ken Nambu Earthquake", Proc. 3rd Kansai International Forum on Comparative Geotechnical Engineering (KIG-Forum '97), pp. 239-248.

Yasuda, S., Ishihara, K., Harada, K. and Nomura, H. (1996), "Area of Ground Flow Occurred behind Quaywalls due to Liquefaction", Proc. of the 3rd Kansai International Forum on Comparative Geotechnical Engineering (KIG-Forum '97), pp. 85-93

Yoshimi, Y., Tokimatsu, K. and Hosaka, Y. (1989), "Evaluation of Liquefaction Resistance of Clean Sands Based on High-Quality Undisturbed Samples" Soils and Foundations, Vol. 29, No.1, pp. 93-104.